

**Gentle Driving of Piles (GDP) at a sandy site combining axial and torsional vibrations  
Part II - cyclic/dynamic lateral loading tests**

Kementzetzidis, Evangelos; Pisano, Federico; Elkadi, Ahmed S.K.; Tsouvalas, Apostolos; Metrikine, Andrei

**DOI**

[10.1016/j.oceaneng.2022.113452](https://doi.org/10.1016/j.oceaneng.2022.113452)

**Publication date**

2023

**Document Version**

Final published version

**Published in**

Ocean Engineering

**Citation (APA)**

Kementzetzidis, E., Pisano, F., Elkadi, A. S. K., Tsouvalas, A., & Metrikine, A. (2023). Gentle Driving of Piles (GDP) at a sandy site combining axial and torsional vibrations: Part II - cyclic/dynamic lateral loading tests. *Ocean Engineering*, 270, Article 113452. <https://doi.org/10.1016/j.oceaneng.2022.113452>

**Important note**

To cite this publication, please use the final published version (if applicable).  
Please check the document version above.

**Copyright**

Other than for strictly personal use, it is not permitted to download, forward or distribute the text or part of it, without the consent of the author(s) and/or copyright holder(s), unless the work is under an open content license such as Creative Commons.

**Takedown policy**

Please contact us and provide details if you believe this document breaches copyrights.  
We will remove access to the work immediately and investigate your claim.



# Gentle Driving of Piles (GDP) at a sandy site combining axial and torsional vibrations: Part II - cyclic/dynamic lateral loading tests

Evangelos Kementzetzidis<sup>a</sup>, Federico Pisanò<sup>a,\*</sup>, Ahmed S.K. Elkadi<sup>b</sup>, Apostolos Tsouvalas<sup>a</sup>, Andrei V. Metrikine<sup>a</sup>

<sup>a</sup> Faculty of Civil Engineering and Geosciences, Delft University of Technology, Stevinweg 1, Delft, 2628 CN, The Netherlands

<sup>b</sup> Deltares, Boussinesqweg 1, Delft, 2629 HV, The Netherlands

## ARTICLE INFO

### Keywords:

Piles & piling  
Soil/structure interaction  
Cyclic loading  
Dynamics  
Pile–soil gapping  
Sands

## ABSTRACT

Gentle Driving of Piles (GDP) is a new technology for the vibratory installation of tubular (mono)piles. Its founding principle is that both efficient installation and low noise emission can be achieved by applying to the pile a combination of axial and torsional vibrations. Preliminary development and demonstration of the proposed technology are the main objectives of the GDP research programme. To this end, onshore medium-scale tests in sand have been performed on piles installed using both impact and vibratory driving methods (including GDP). While the results of the installation tests are presented by Tsetas et al. (2023), this work focuses on the post-installation performance of GDP-driven piles under a sequence of slow/large-amplitude (cyclic) and faster/low-amplitude (dynamic) load parcels. The field data point out the influence of onshore unsaturated soil conditions, which result in complex cyclic pile stiffness trends due to the interplay of pile–soil gapping and soil's fabric changes. The pile stiffness under small-amplitude vibrations is strongly correlated with the previous response to large load cycles, and noticeably frequency-dependent for load cycles with a period lower than 1 s. Overall, the post-installation performance of GDP-driven piles appears to be satisfactory, which encourages further development and demonstration at full scale.

## 1. Introduction

Ever more countries worldwide are working to shift their energy mix towards renewables. The Netherlands, country of origin of this study, is actively contributing to the European decarbonisation agenda (European Commission, 2020) by promoting the exploitation of renewable energy sources, both onshore and offshore (Minister of Economic Affairs and Climate Policy, 2020). In the country, recent policy updates require a substantial increase in offshore wind capacity to 4.5 GW by 2023 and to 21 GW by 2030 (Dutch Government, 2022). In this regard, offshore wind energy will continue to play an increasingly relevant role as an abundant, cost-effective resource (Esteban et al., 2011), on the condition that the pace of its technological development is further expedited. Presently, 15%–24% of the investment for the construction of an offshore wind farm relates to the design, production, and installation of substructures (Stehly and Beiter, 2020). Continual improvement of engineering methodologies in this area is therefore key to achieving further cost reduction (Byrne et al., 2019; Page et al., 2019; Wu et al., 2019; Pisanò et al., 2022a,b).

As reported in the latest EWEA report (Ramírez et al., 2021), over 80% of the existing offshore wind turbines (OWTs) in European

wind farms are founded on so-called monopile foundations, which are most commonly installed by means of impact hammering. The impact technology is to date very well established in the offshore industry (Kallehave et al., 2015). However, impact installation in certain soil conditions (e.g., dense sands) may be slower than desired (Rodger and Littlejohn, 1980; Achmus et al., 2020), which causes increased installation costs and, possibly, higher pile damage under many hammer blows (Mosher, 1987; Meijers et al., 2018). Moreover, the underwater noise emitted during pile installation is known to be harmful to marine life, and has motivated over the years the enforcement of strict regulations to limit its negative environmental effects (Tsouvalas, 2020). Such regulations include the adoption of costly soundproofing measures (Koschinski and Lüdemann, 2013; Tsouvalas and Metrikine, 2016a).

An interesting alternative to impact piling is provided by vibratory technologies, which can achieve quiet(er)/fast pile installation through the application of low-amplitude axial vibrations. The input excitation is induced through the harmonic rotation of eccentric masses, usually at a frequency no larger than 40 Hz. Vibratory pile hammers (or simply

\* Corresponding author.

E-mail address: [f.pisano@tudelft.nl](mailto:f.pisano@tudelft.nl) (F. Pisanò).

### List of acronyms and symbols

ATP	Auxiliary test pile
CPTu	Cone penetration testing with pore water pressure measurement
CSL	Crosshole sonic logging
DSI	Detailed site investigation
FBG	Fiber Bragg grating sensors
GDP <sub>1</sub> , GDP <sub>2</sub>	Piles installed via GDP driving
GDP <sub>01</sub> , GDP <sub>02</sub>	Auxiliary piles installed via GDP driving
GDP	Gentle Driving of Piles
HPT-MPT	Hydro-profiling tests with mini pump tests
IH	Pile installed via impact hammering
MTP	Main test pile
PPT	Pore water pressure transducers
PSI	Preliminary site investigation
SCPTu	Seismic cone penetration testing with pore water pressure measurement
SPC	Soil pressure cell
VH	Pile installed via axial vibratory driving
$ K_{dyn} $	Absolute value of the dynamic stiffness
$D$	Pile diameter
$D_r$	Relative density
$E_D$	Stored elastic energy
$F$	Load
$F_{av}$	Average pile load
$F_{cyc}$	Cyclic pile load
$\hat{F}$	Normalised pile load
$f$	Frequency
$h$	Pile wall thickness
$K_0$	Static tangential stiffness

$K_{cyc}^{av}$	Average secant cyclic stiffness
$K_{cyc}^{cg}$	Closed-gap tangential cyclic stiffness
$K_{cyc}^{og}$	Open-gap tangential cyclic stiffness
$K_{cyc}^{tan}$	Tangential cyclic stiffness
$k_h$	Horizontal hydraulic conductivity
$E_S$	Plastic work
$L$	Pile length
$L_e$	Embedded pile length
$L_x$	Pile–soil gap breadth
$L_y$	Pile–soil gap depth
$L_{x,max}$	Maximum pile–soil gap breadth
$N$	Number of cycles
$p_a$	Atmospheric pressure
$p_w$	Pore water pressure
$q_c$	Cone penetration resistance
$t$	Time
$U$	Pile displacement
$\bar{U}$	Normalised pile displacement
$V_s$	Shear wave velocity
$z$	Soil depth coordinate (under ground surface)
$\Delta\sigma_r$	Variation of radial soil stress
$\Delta p_w$	Variation of pore water pressure
$\gamma'$	Soil's buoyant unit weight
$\sigma_r$	Radial soil stress

'vibro-hammers') have been manufactured since the 1940s (Rodger and Littlejohn, 1980), and their benefits in terms of driving/noise performance already put in evidence by a number of previous studies (Barkan, 1967; Mosher, 1987, 1990; Lammertz, 2003; Tsouvalas and Metrikine, 2016b). The use of piling loads lower than in impact driving can effectively reduce both the damage and the radial expansion of the pile during driving — the latter (Poisson effect) is a major culprit for noise emission and larger soil resistance to driving (De Nicola and Randolph, 1993). Despite its obvious benefits, vibratory driving is not yet widely adopted for offshore piling. Its use is hindered by a number of factors, including the limited availability of field data. Major knowledge gaps also exist regarding the dynamic behaviour of the soil during vibro-driving (Mazza and Holeyman, 2019) and the effects of vibro-installation on the operational performance of the pile (Anusic et al., 2019; Tsetas et al., 2020; Achmus et al., 2020; Staubach et al., 2022; Kementzetzidis, 2023).

To boost the improvement of vibro-piling methods, a new technology – Gentle Driving of Piles (GDP) – has been recently proposed in the Netherlands as core of a joint industry project led by the Delft University of Technology (TU Delft) (Metrikine et al., 2020). GDP targets enhanced piling performance and reduced noise emissions through the simultaneous application of low-frequency/axial and high-frequency/torsional vibrations. This thread of research was originally inspired by observing that torsional vibrations do not induce radial pile expansion during driving, which was foreseen to play in favour of both driving and acoustic performances. A preliminary demonstration of the proposed technology was pursued by performing medium-scale field tests on identical test piles installed using impact and vibratory driving methods, including GDP. The tests were performed in sandy

soil at the Port of Rotterdam and comprised two distinct stages, the first to investigate the driving performance, and the second to explore installation effects in the response of the test piles to repeated lateral loading.

While the rationale and early development of the GDP technology is discussed in the companion paper by Tsetas et al. (2023), this paper focuses on the post-installation response of the test piles to cyclic/dynamic lateral loading. In particular, the behaviour observed for two GDP-driven piles is thoroughly discussed in light of the geotechnical conditions encountered at the test site. Selected field measurements are presented in the following to (i) 'reassure' future users about the cyclic/dynamic performance of GDP-driven piles, and (ii) establish a conceptual framework for the interpretation of the whole field data set.

Although the GDP project was originally motivated by offshore wind developments, this paper provides experimental evidence and conceptual findings that are generally relevant to piled foundations, repeated lateral loading, and onshore sandy site conditions.

## 2. Medium-scale field tests at the Maasvlakte II site

The response of piles to monotonic lateral loading has been researched since the 1960s (McClelland and Focht, 1956; Matlock and Reese, 1962; Matlock, 1970; Poulos, 1971; Reese et al., 1975; Poulos and Davis, 1980). The interest for dynamic loading conditions was later motivated by earthquake engineering applications, and was initially limited to the derivation of dynamic impedance functions for slender piles (Novak, 1974; Kagawa and Kraft, 1980; Angelides and Roesset, 1981; Gazetas and Dobry, 1984; Dobry and Gazetas, 1988; Mylonakis and Gazetas, 1999; Shadlou and Bhattacharya, 2014). Only more recently, this line of work has been extended to the case of short/stiff offshore units (monopiles and caissons) (Shadlou and Bhattacharya, 2016; He et al., 2019), though without considering relevant non-linear effects, such as gradual variations in lateral stiffness and cyclic accumulation of pile rotation (also termed 'tilt'). The latter aspect has



Fig. 1. GDP test site and its access routes — edited after (OpenStreetMap contributors, 2017).

Table 1

Pile dimensions.

		Test piles	Reaction pile
Length	$L$	10 m	10 m
Embedded length	$L_e$	8 m	8 m
Outer diameter	$D$	0.762 m	1.6 m
Wall thickness	$h$	0.0159 m	0.02 m

attracted particular attention in the context of offshore wind research, since limiting the monopile tilt during the whole operational life has been recognised as an important design criterion (Arany et al., 2017). A number of experimental studies have been performed to investigate the occurrence and evolution of cyclic monopile tilt, including small-scale tests under normal (1g) (LeBlanc et al., 2010; Abadie, 2015; Albiker et al., 2017; Frick and Achmus, 2019; Richards, 2019) or augmented gravity (Klinkvort et al., 2010; Klinkvort, 2012; Rudolph et al., 2014; Zhu et al., 2016; Wang et al., 2018; Truong et al., 2019; Richards et al., 2021), as well as medium-scale tests in the field (Li et al., 2015; Byrne et al., 2020a,b).

The GDP field tests were performed at the Maasvlakte II port site in Rotterdam, which comprises North Sea sand that was used to create a reclaimed/compacted site. Site location and access routes are shown in Fig. 1; the accessibility of the site and its proximity to logistic suppliers were relevant criteria in the site selection process.

### 2.1. Test layout and site investigation

Geotechnical investigation activities at the Maasvlakte II site were carried out between June and September 2019 in two phases of *preliminary* and *detailed* site investigation — henceforth referred to as PSI and DSI, respectively. In October/November 2019, nine tubular steel piles were installed: eight test piles, and a larger/stiffer reaction pile for the post-installation loading tests (pile specifications in Table 1). Four of the test piles, henceforth referred to as *Main Test Piles* (MTPs), were extensively instrumented, while the other four piles, labelled as *Auxiliary Test Piles* (ATPs), were installed uninstrumented for preliminary testing purposes. The four MTPs were installed and labelled after the corresponding driving method, namely impact hammering (IH), axial vibro-hammering (VH), and GDP-driving ( $GDP_{1,2}$ ), whereas the ATPs were installed via impact hammering ( $IH_{01,02}$ ) and GDP-driving ( $GDP_{01,02}$ ). As shown in Fig. 2, the MTPs and the ATPs were installed around the reaction pile at a radial, centre-to-centre distance of 12 m and 16 m, respectively.

Relevant site investigation work is summarised in what follows, with further details provided by Tsetas et al. (2023). First, the PSI was performed to identify suitable locations for installing the test piles, mostly in light of site homogeneity and pile spacing considerations. During the PSI, 25 CPTu tests were performed down to a target depth of 10 m over a regular grid with a spacing of about 12.5 m. The PSI also enabled the identification of the water table depth — between 3.5 and 4.5 m below the ground surface, depending on the specific location. After selecting the final pile locations (Fig. 2), the DSI was carried out around and at the centre of all piles. The DSI programme included:

- four CPTu tests at the ATP locations (target depth: 10 m);
- four Seismic CPTu (SCPTu) tests at the MTP locations (target depth: 10 m);
- four hydro-profiling tests with mini pump tests (HPT-MPT) around the MTPs (target depth: 15 m);
- borehole sampling around the MTPs, with a total of eight 10 m long boreholes (two per MTP);
- crosshole sonic logging (CSL) tests performed at MTP locations before and after pile driving (Tsetas et al., 2023).

Both PSI and DSI data confirmed the predominantly sandy nature of the soil deposit from the ground surface down to approximately 10 m below. The upper 5 m consist of the dredged material employed to create the Maasvlakte II site, which overlays a layer of sand and clayey/silty sand from the Holocene Naaldwijk formation (Vos, 2015). With reference to the locations of the MTPs and the GDP ATPs, the profiles in Fig. 3 of (a) cone resistance ( $q_c$ ), (b) shear wave velocity ( $V_s$ ), and (c) relative density ( $D_r$ ) (based on Jamiolkowski et al., 2003) suggest the presence of medium-dense to very dense sand ( $D_r = 60\text{--}100\%$ ) with an overall negative  $D_r$  depth-gradient. The same negative gradient is also exhibited by the corresponding SCPTu profiles of  $V_s$  (only available for the MTP locations). Profiles of hydraulic conductivity ( $k_h$ , horizontal component) are reported in Fig. 3(d) after HPT-MPT measurements close to the locations of the MTPs. The  $k_h$  values shown in the figure lie mostly in the range of  $10^{-4}\text{--}10^{-3}$  m/s (average permeability of  $4.45 \times 10^{-4}$  m/s over the first 10 m.), which is typical for the sandy soil found at the Maasvlakte II site. Since the interpretation of HPT-MPT tests relies on the assumption of water-saturated soil, it was not attempted to infer  $k_h$  values for the unsaturated soil above the water table.

### 2.2. Pile instrumentation, ground monitoring, and loading equipment

The mechanical response of the instrumented MTPs was recorded by means of the following sensors — technical specifications provided by Tsetas et al. (2023):

- fiber Bragg grating (FBG) sensors at multiple locations along the piles, to monitor strains in the longitudinal and two inclined directions, at angles of 60 and 120 degrees with respect to the horizontal axis;
- two triaxial accelerometers installed at diametrically opposite locations, to record the dynamic response of the piles during installation;
- one potentiometer transducer, to record the progress of pile penetration by measuring the vertical displacement;
- one temperature sensor placed 40 cm above the pile tip.

Ground sensors were also installed to enable deeper understanding of pile–soil interaction mechanisms. Eight VWPC2100 *RST Instruments* sensors containing both soil pressure cells (SPCs) and pore water pressure transducers (PPTs) were deployed to simultaneously record the evolution in time of the total radial stress ( $\sigma_r$ ) and the pore pressure ( $p_w$ ), with accuracy and resolution of 5 kPa and 0.25 kPa, respectively. For each MTP and prior to pile driving, the sensors were installed at two different depths (6 m and 8 m below the ground surface, see Fig. 2) and

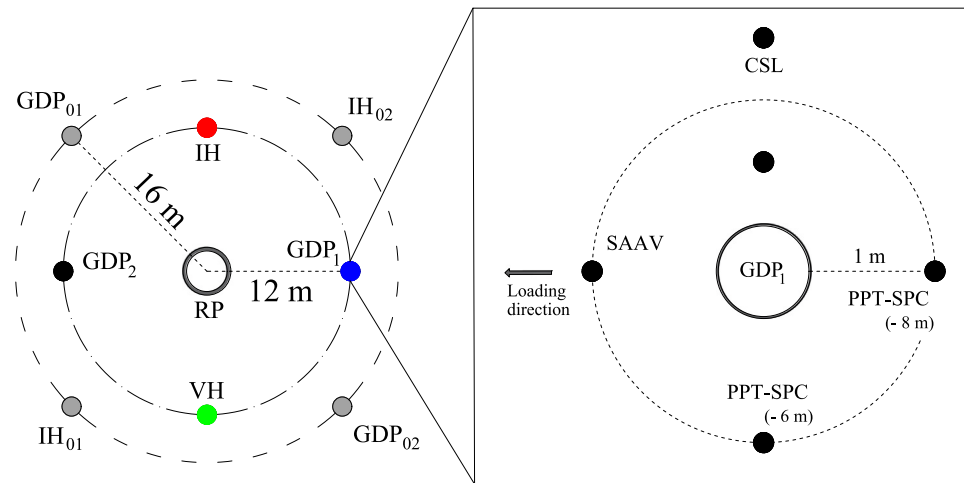


Fig. 2. Site layout (left — ATPs in grey) and soil monitoring around the MTPs (right). For better readability, the site layout on the left is shown with MTP diameters and distances from the central RP that are not to scale.

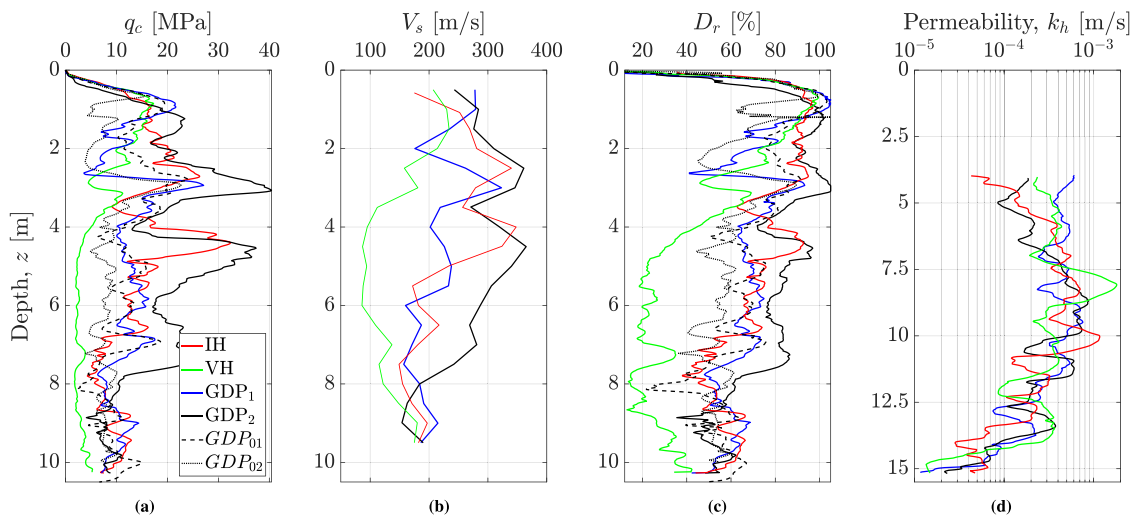


Fig. 3. Profiles of (a) cone resistance ( $q_c$ ), (b) shear wave velocity ( $V_s$ ), (c) relative density ( $D_r$ ), and (d) horizontal hydraulic conductivity ( $k_h$ , 80 cm moving average plot).  $q_c$  and  $D_r$  obtained from CPTs performed on all piles while  $V_s$  and  $k_h$  available only at the MTP locations from in-situ SCPTu and HPT-MPT tests.

set to record with a sampling frequency of 100 Hz. All load test data were low-pass filtered at 12 Hz to remove high-frequency noise from the measurements.

The lateral loading tests, main subject of this paper, were performed using the loading frame illustrated in Fig. 4. The loading equipment included a TU Delft servo-hydraulic jack, which was able to impose load-controlled horizontal forcing by means of a closed-loop control system. The servo-hydraulic jack could load the test piles through the tension of the connection beam, i.e., by cyclically pulling test and reaction piles towards each other at a specified loading frequency. A custom-built load cell was also employed to ensure the application of desired load amplitudes regardless of the relative deflection of the opposite piles. The load cell provided highly repeatable load values over a selected range of 0.8 MN, with accuracy and resolution of 0.25 kN and 0.015 kN, respectively.

Since all test piles were installed to a target depth of 8 m, the remaining pile length allowed lateral loading with an eccentricity  $e = 1$  m above the ground surface. During lateral loading, the deflection of all test piles was sampled and low-pass filtered at 6789 Hz and 70 Hz, respectively, via the displacement sensors (Gefran PY1, 100 mm stroke) shown in Fig. 5.

As previously mentioned, four piles in total (GDP piles) were installed through the GDP vibratory method. The testing programme

comprised monotonic loading on the non-instrumented GDP ATPs (GDP<sub>01</sub> and GDP<sub>02</sub> in Fig. 2) and multi-amplitude cyclic/dynamic loading on the four instrumented MTPs. Particularly, the latter tests were conceived to explore the lateral response of the test piles to combinations of slow/large-amplitude (cyclic) and fast(er)/small-amplitude (dynamic) loading. Henceforth, the terms ‘cyclic’ and ‘dynamic’ are used to distinguish these two types of loading parcels and the associated pile response.

### 2.3. Preliminary monotonic tests

Preliminary monotonic tests were carried to support the definition of a cyclic loading programme compatible with the capabilities of the loading frame. Monotonic loading was applied to the two GDP ATPs as is shown on the right-hand side of Fig. 6(a) (load vs time), while the resulting force–displacement responses are reported on the left — the pile displacement at the ground level was assumed to coincide with the output of sensor 4 in Fig. 5. The load was kept constant on both ATPs after achieving the intended maximum value of 550 kN, while additional constant-load stages were introduced for GDP<sub>02</sub> (at 325 kN and 400 kN) to allow for possible creep deformations. The presence of rate effects in the monotonic pile response was evaluated for GDP<sub>01</sub> by varying the loading rate with respect to the main selected value of 0.05

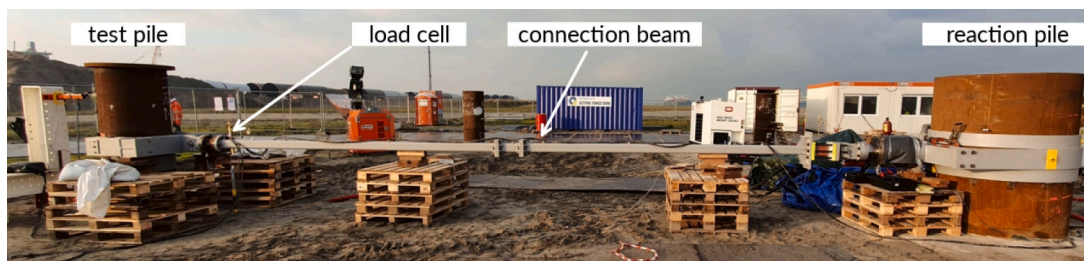


Fig. 4. The loading frame connecting a test pile (left) to the reaction pile (right). The wooden supports in the picture were used to counteract the vertical deflection of the connection beam under its own self-weight.

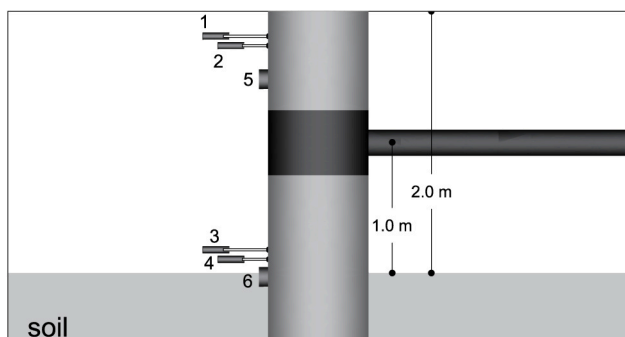


Fig. 5. Lateral pile motion monitoring by means of displacement sensors (1–2, 3–4) and inclinometers (5–6). The pile displacement at the ground surface was assumed to approximately coincide with the output of sensor 4 located for all piles approximately 15 cm above the ground.

kN/s. During the test on GDP<sub>01</sub> the loading rate was increased twice to 70 kN/s, namely when the applied load lied in the ranges of 0–180 kN and 330–420 kN. The fastest loading rate of 70 kN/s was selected as representative of the average rate that the MTPs would later experience under the cyclic loading parcel of largest amplitude.

Due to technical limitations of the loading frame, it was not possible to load the two piles up to their (conventional) capacity — e.g., associated with a lateral deflection of  $0.1D$  at the ground surface. Such a capacity was thus estimated by analytically extrapolating the monotonic response (see the dashed interpolation line in Fig. 6(a)). For instance, a conventional capacity of 1.46 MN was estimated for GDP<sub>01</sub> and a loading rate of 0.05 kN/s.

The lateral response of GDP<sub>01</sub> was found indistinguishable to that of the GDP<sub>02</sub>, at least during the onset of lateral loading highlighting relevant installation effects as discussed in Kementzetzidis (2023). Towards higher loads, GDP<sub>01</sub> appears to be globally stiffer than GDP<sub>02</sub>'s, which is consistent with the values of cone resistance at the two pile locations (cf. to Fig. 3). The clear presence of both rate effects and creep in the measured pile responses confirms that time effects can be significant even in sandy soil (Lazari et al., 2019). It should also be noted that the same field evidence might have been co-promoted by the occurrence of transient hydromechanical processes in the shallow unsaturated soil. While more field research on this subject is being carried out (Buckley et al., 2020), an influence of time effects is generally to be expected.

The same monotonic responses in Fig. 6(a) are re-plotted in Fig. 6(b) left after normalising the applied load ( $\bar{F} = F/L_e^2 D \gamma'$ ) and the displacement ( $\bar{U} = U/D \cdot \sqrt{\rho_a/L_e \gamma'}$ ) as proposed by LeBlanc et al. (2010). Such a normalisation enables some comparison to selected field test results from the PISA project (McAdam et al., 2020), particularly to those associated with piles DS4 ( $L_e/D = 10$ ,  $D = 0.273$  m,  $h = 0.7$  cm,  $e = 10$  m) and DM3 ( $L_e/D = 8$ ,  $D = 0.762$  m,  $h = 2.5$  cm,  $e = 10$  m) — cf. to the GDP pile specifications in Table 1. Although GDP<sub>01,02</sub> and DS4/DM3 share similar  $L_e/D$  ratios, a totally fair comparison between

the corresponding lateral responses does not seem to be possible, due to the differences in load eccentricity and soil profile — recent work on more general normalisation strategies has successfully dealt with the former, but not yet with the latter (Wang et al., 2022). Nevertheless, reasonable agreement between the two sets of field data is observed, which is encouraging from a general validation perspective — see also the magnified view around small displacements in Fig. 6(b)-right.

#### 2.4. Cyclic/dynamic loading programme

The cyclic/dynamic loading programme applied to the MTPs is illustrated in Fig. 7. Each cyclic/dynamic test lasted about 40 h and included a total amount of  $N = 82000$  loading cycles. Some of the cycles were applied with relatively large amplitude at constant/low frequency (black parcels in Fig. 7), with interleaved stages of small-amplitude loading at variable frequency (henceforth referred to as dynamic ‘frequency sweeps’ — grey parcels in Fig. 7). All load parcels were defined by combining a monoharmonic excitation of amplitude  $F_{cyc}$  and frequency  $f$  with an average load level  $F_{av}$ :

$$F(t) = F_{av} + F_{cyc} \times \sin(2\pi ft) \quad (1)$$

All the loading settings associated with Eq. (1) and Fig. 7 are summarised in Table 2. Cyclic/dynamic loading was applied in all instances with  $F_{av} > F_{cyc}$  (‘one-way’ loading), therefore with no risk of compression buckling for the connection beam in Fig. 4. The stroke (displacement range) of the loading frame was limited by the capabilities of the hydraulic power unit, which finally allowed for a maximum load of 350 kN when applied at 0.1 Hz, and a maximum loading frequency of 4 Hz.

Each low-frequency cyclic parcels ( $a - e$  in Fig. 7) comprised  $N = 1000$  cycles. Taking GDP<sub>01</sub>'s CPT profile as an average of the profiles at all MTPs locations, the aforementioned reference capacity of 1.46 MN was retained for both GDP-driven MTPs as a reasonable first approximation. Accordingly, the maximum load magnitudes ( $F_{av} + F_{cyc}$ ) imposed during the parcels  $a-d$  and  $b-c-e$  were, respectively, 12% and 24% of the reference capacity — these are representative of operational loading conditions for modern OWT monopiles (Kementzetzidis et al., 2019), and also sufficient to mobilise non-linear features of pile–soil interaction. Such features include, e.g., the cyclic accumulation of permanent pile displacement, which is closely related to the perturbation of the stress state and micro-structure of the surrounding soil (Cuéllar et al., 2009). In order to mitigate creep effects in the cyclic response, every change towards new  $F_{av} - F_{cyc}$  pairs was preceded by a 10 min stage of static preloading — see the magnified window in Fig. 7.

Dynamic frequency sweeps (or f-sweeps, for brevity) were interleaved between consecutive cyclic parcels (Fig. 7) to gain insight into the response of the test piles during weak vibrations and for different  $F_{av}$  values; the possible impact on the (dynamic) lateral stiffness of a varying loading frequency was also inspected in light of the full-scale observations discussed by Versteijlen et al. (2017) and Kementzetzidis et al. (2021). The 16 frequency sweeps featured  $N = 4800$  cycles applied at a constant/low amplitude of  $F_{cyc} = 2.5$  kN, while the loading

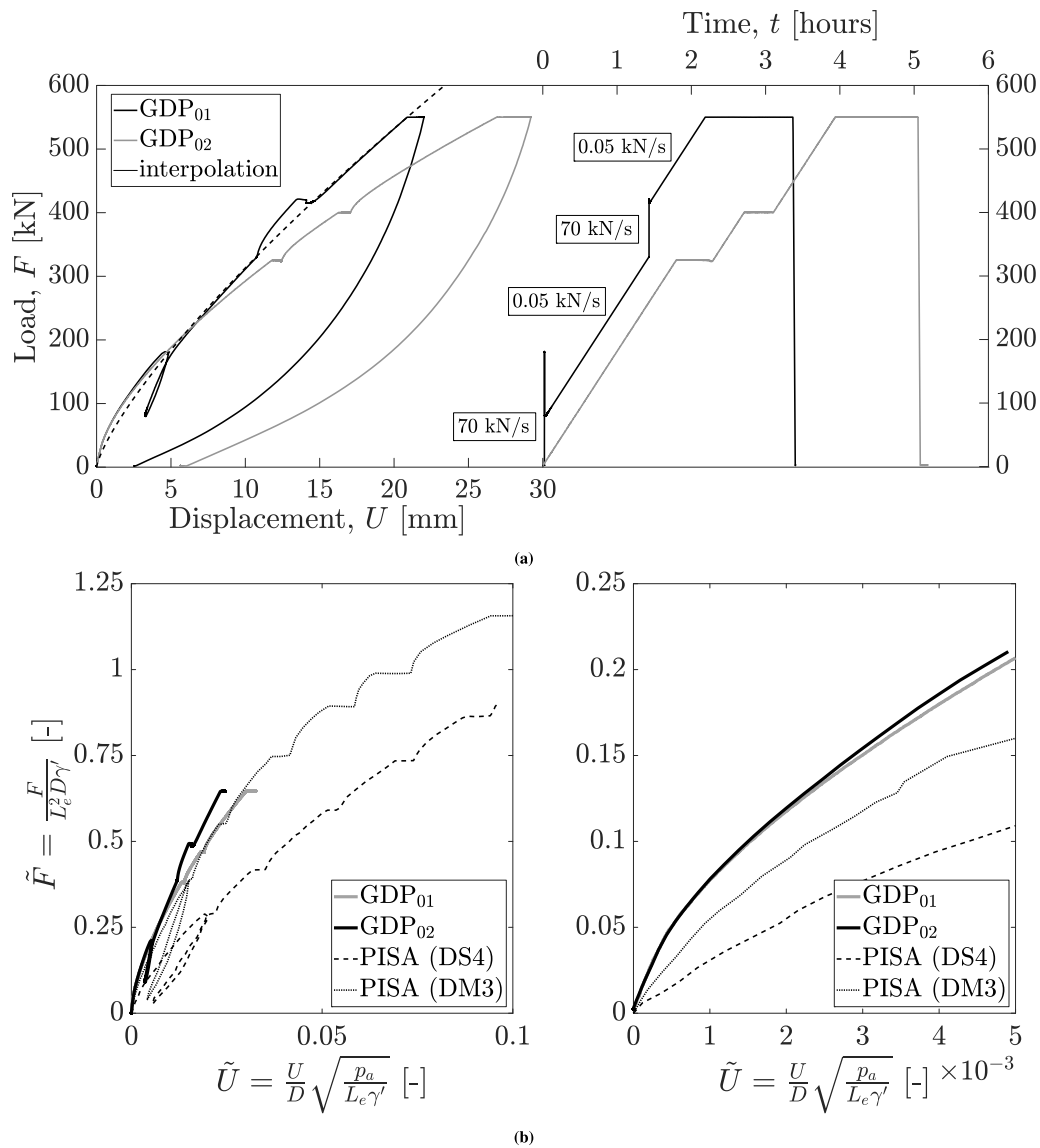


Fig. 6. (a) Monotonic loading test results for the ATPs GDP<sub>01</sub> and GDP<sub>02</sub>; (b) comparison in terms of normalised load ( $\tilde{F}$ ) and displacement ( $\tilde{U}$ ) between the monotonic responses of GDP<sub>01</sub>–GDP<sub>02</sub> and those of the piles DS4 ( $L_e/D = 10$ ,  $D = 0.273$  m,  $h = 0.7$  cm) and DM3 ( $L_e/D = 8$ ,  $D = 0.762$  m,  $h = 2.5$  cm) tested in the framework of the PISA project (McAdam et al., 2020): (left) full test view and (right) magnified view of the small-displacement range.  $p_a$  and  $\gamma'$  stand in the normalisation for atmospheric pressure and buoyant soil unit weight, respectively.

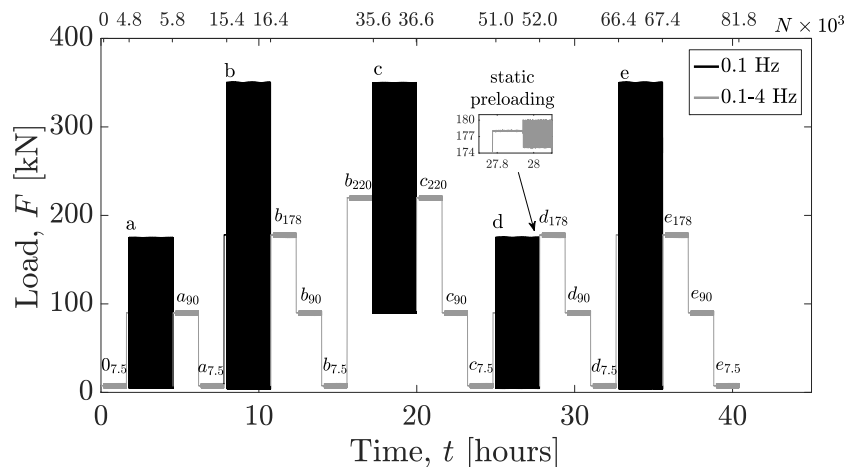
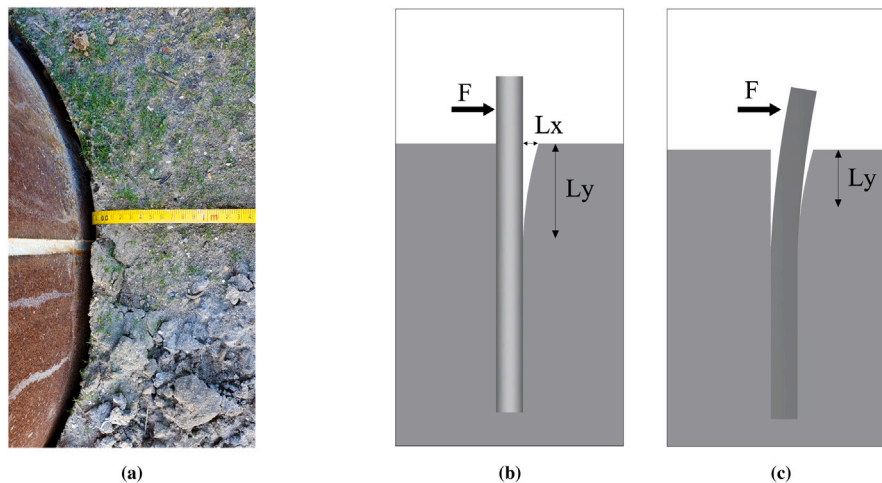


Fig. 7. Cyclic/dynamic loading programme. Load amplitudes are provided against time (bottom axis) and number of cycles (top axis). Cyclic load parcels (a – e) and dynamic f-sweeps (a – e) are shown in black and grey, respectively — see loading specifications in Table 2.

**Table 2**  
Loading specifications for the cyclic/dynamic field tests — cf. to Fig. 7.

–	$F_{av}$ [kN]	$F_{cyc}$ [kN]	$f$ [Hz]	$N \times 10^3$	–	$F_{av}$ [kN]	$F_{cyc}$ [kN]	$f$ [Hz]	$N \times 10^3$
$0_{7.5}$	7.5	2.5	0.1–4	4.8	$c_{90}$	89.5	2.5	0.1–4	4.8
<b>a</b>	<b>90</b>	<b>85</b>	<b>0.1</b>	<b>1</b>	$c_{7.5}$	7.5	2.5	0.1–4	4.8
$a_{90}$	89.5	2.5	0.1–4	4.8	<b>d</b>	<b>90</b>	<b>85</b>	<b>0.1</b>	<b>1</b>
$a_{7.5}$	7.5	2.5	0.1–4	4.8	$d_{178}$	177.5	2.5	0.1–4	4.8
<b>b</b>	<b>177.5</b>	<b>172.5</b>	<b>0.1</b>	<b>1</b>	$d_{90}$	89.5	2.5	0.1–4	4.8
$b_{178}$	177.5	2.5	0.1–4	4.8	$d_{7.5}$	7.5	2.5	0.1–4	4.8
$b_{90}$	89.5	2.5	0.1–4	4.8	<b>e</b>	<b>177.5</b>	<b>172.5</b>	<b>0.1</b>	<b>1</b>
$b_{7.5}$	7.5	2.5	0.1–4	4.8	$e_{178}$	177.5	2.5	0.1–4	4.8
$b_{220}$	219.5	2.5	0.1–4	4.8	$e_{90}$	89.5	2.5	0.1–4	4.8
<b>c</b>	<b>220</b>	<b>130</b>	<b>0.1</b>	<b>1</b>	$e_{7.5}$	7.5	2.5	0.1–4	4.8
$c_{220}$	219.5	2.5	0.1–4	4.8					



**Fig. 8.** (a) Pile–soil gap observed after loading monotonically an ATP; pile–soil contact patterns after first gap formation (i.e., for  $N > 1$ ): (b)  $F = 0$  (fully unloaded pile), and (c)  $F > 0$  (during pile reloading).

frequency was increased from 0.1 Hz to 4 Hz with increments of 0.1 Hz every 120 cycles. Preliminary tests on the ATPs indicated that 120 cycles would be generally sufficient for the attainment of a steady-state response under the considered loading/site conditions.

In what follows, individual dynamic parcels are referred to as labelled in Fig. 7 — for example,  $b_{7.5}$  denotes a frequency sweep applied after the cyclic parcel  $b$  around an average load of 7.5 kN, while ‘ $f_b$ -sweeps’ indicates the whole set of frequency sweeps between parcels  $b$  and  $c$ .

### 3. Pile response to cyclic load parcels

This section elaborates on the results of the tests performed on the GDP MTPs, particularly on the response to slow/large amplitude load parcels ( $a - e$  in Fig. 7).

#### 3.1. Impact of onshore soil conditions

As confirmed by previous field studies (Li et al., 2015; Achmus et al., 2020; McAdam et al., 2020), onshore tests are typically affected by the presence of shallow unsaturated soil. An important consequence of unsaturated soil conditions is the development of an apparent cohesion, even in otherwise cohesionless soils such as sands (Fredlund, 2006). Such a cohesion allows sand to self-sustain, and therefore enables the formation of a vertical soil–pile gap during lateral loading — see in Fig. 8(a) an example of soil–pile gap observed at the GDP site. Gapping introduces a geometrical non-linearity in the lateral behaviour of a pile, in that its embedment in the soil (in full contact) becomes a function of the lateral displacement (Figs. 8(b)–8(c)). The formation and evolution of the gap impacted significantly the cyclic/dynamic pile

response during the whole loading programme, however in a manner not expected at offshore sites.

Fig. 9(a) displays the cyclic load–displacement response of GDP<sub>2</sub> to the cyclic load parcel  $a$  in Fig. 7, with emphasis on  $N = 1, 2, 1000$ . The effect of the gap emerges immediately from the comparison between the responses measured during the first two cycles: while a typical decrease in tangent stiffness with the load amplitude is observed during the former, an opposite (*locking*) behaviour is observed during the latter and magnified by prolonged cycling — cf. to  $N = 1000$ . This finding is further supported by Fig. 9(b), which displays GDP<sub>2</sub>'s force–displacement response to the five cyclic load parcels (from  $a$  to  $e$ ). The response during the first two cycles is qualitatively very similar for parcels  $a$  and  $b$ , whereas only a stiffening behaviour is observed for the following parcels  $c - d - e$  from the onset of loading. It may thus be inferred that the geometry of the gap mainly evolved during the first cycles of parcels  $a$  and  $b$ . In this respect, the interaction between lateral pile behaviour and gap formation/evolution can be simply conceptualised with the aid of Fig. 8, where  $L_y$  and  $L_x$  denote, respectively, the current depth and opening of the gap on one side of the pile (Fig. 9(a)). It may be argued that the maximum value of  $L_x$ ,  $L_{x,max}$ , approximately coincides with the largest displacement ever experienced by the pile (minus the soil rebound caused by elastic unloading Matlock et al., 1978), which evolves in time depending on the specific features of the loading sequence (Fig. 7). Upon unloading (i.e., reversal of the load direction), the apparent soil cohesion allows soil–pile separation with a (nearly) vertical soil wall; upon the subsequent reloading, the pile regains contact with the self-standing soil wall after moving through the open gap. As the gap progressively recloses (i.e.,  $L_x$  and  $L_y$  decrease), the deflection of the pile is resisted by an increasing mass of ‘engaged’ soil, which produces the gradual stiffening of lateral response (tangent stiffness) that is visible in Figs. 9(a)–9(b) for  $N > 1$ . Generally, the

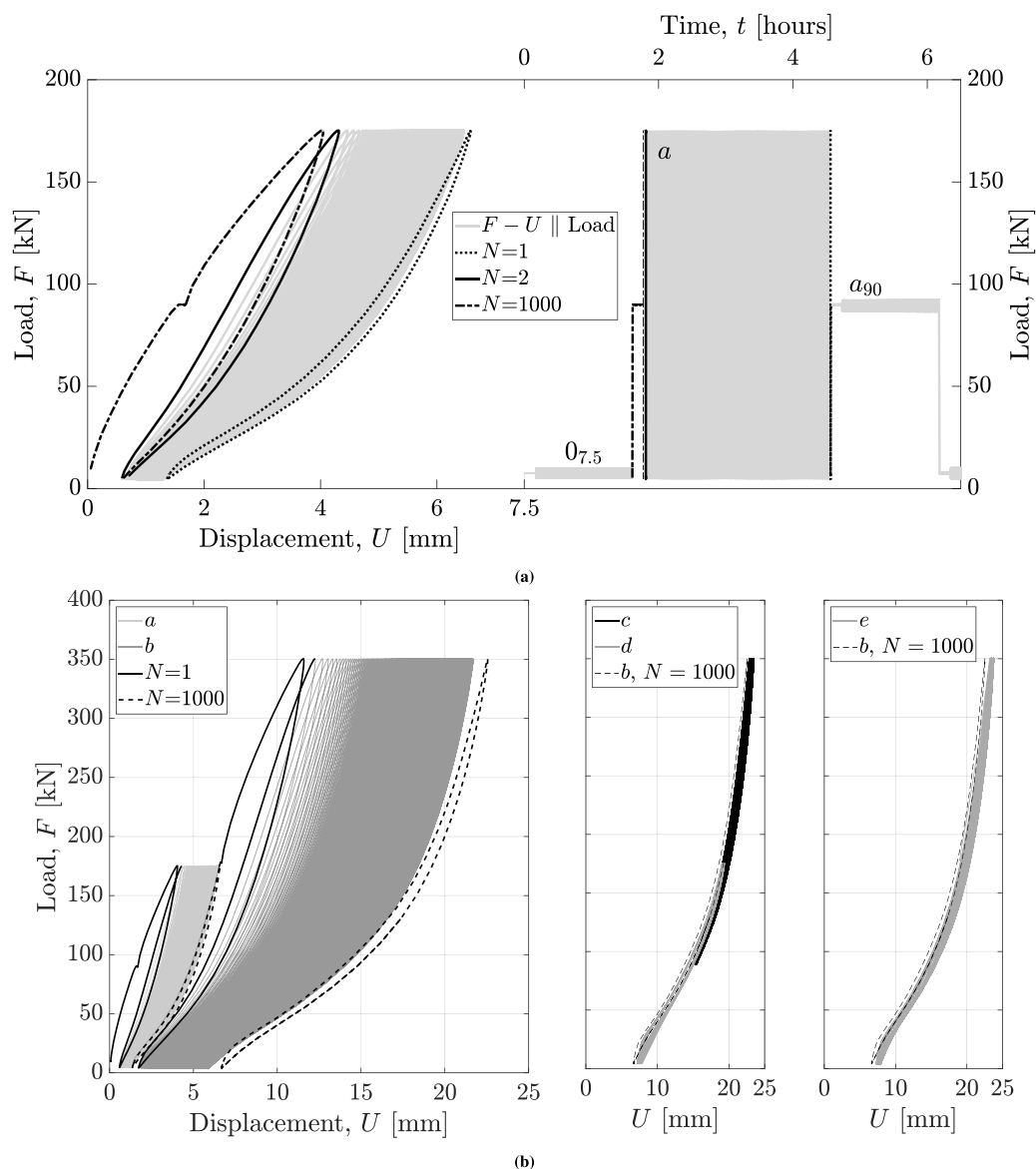


Fig. 9. (a) GDP<sub>2</sub>'s load–displacement response to the first cyclic load parcel (a) in Fig. 7 (left), and the corresponding load-time history (right); (b) GDP<sub>2</sub>'s load–displacement response to cyclic load parcels a–b (left), b–c–d (centre), and b–e (right) — solid and dashed black lines highlight the first ( $N = 1$ ) and the last ( $N = 1000$ ) response cycles for parcels a–b.

evolution in time of the gap size is mainly determined by the magnitude of the capillary forces in the unsaturated soil and the maximum loading amplitude experienced by the pile, with only marginal gap enlargement caused by the cyclic lateral ratcheting of the pile. In conclusion,  $L_x$  and  $L_y$  are expected to vary substantially when the cyclic loading amplitude rises to a new maximum as suggested by Figs. 9(b), 11.

It is also apparent in Fig. 9(b) that, due to the gapping mechanism, the resulting cyclic response does not comply with the well-known Masing idealisation, which is at variance with the experimental evidence normally associated with pile tests in either dry or water-saturated sand Abadie (2015) and Liu et al. (2022).

### 3.2. Cyclic pile deflection and bending

Despite the differences in soil profile (Fig. 3), it is possible to draw a qualitative picture of the installation effects associated with different pile driving methods — more quantitative conclusions have recently been obtained by Kementzetzidis et al. (2023), Kementzetzidis (2023) through numerical modelling work, using a novel 1D soil reaction

model accounting both for ratcheting and gapping effects (Kementzetzidis et al., 2022). To this end, Fig. 10(a) shows for all MTPs the evolution in time of the lateral displacement in response to the whole cyclic/dynamic loading sequence. Overall, the GDP-installed piles experienced a smaller deflection than the other piles (cf. GDP<sub>1</sub> to IH considering their similar soil profiles), which reflects positively on the GDP method also from a post-installation perspective. In particular, GDP<sub>2</sub> displaced less than GDP<sub>1</sub>, as one could have anticipated based on the respective CPT profiles. It is also worth noting that the VH-installed pile displaced less than the IH pile, which is rather surprising in light of the pre-installation soil conditions at the respective locations (Fig. 3) — see Tsetas et al. (2023). In this regard, previous studies on full scale monopiles (Achmus et al., 2020) in sand have shown that the installation settings of standard axial vibro-driving can drastically impact the post-installation lateral response in comparison to impact-hammered piles, which seems indeed consistent with the experimental findings of this field study.

It was qualitatively observed for all MTPs that, after the main gap-forming events (parcels a–b), cycling with a lower amplitude

(e.g., parcel *d*) determined a motion of the piles that was entirely within the breadth of the gap (Fig. 8(c)) and, therefore, with a lower cyclic stiffness due to the reduced embedment. As a consequence, wider ranges of cyclic displacement were recorded for a given load parcel when applied under ‘fully gapped’ conditions — compare the pile responses to parcels *a* and *d* in Fig. 10(a). With further reference to parcel *d*, some displacement relaxation was measured, which indicates a reversal in the direction of pile deflection. Such a mechanism, sometimes termed *self-healing* or *stabilisation*, was first documented in relation to small-scale 1 g tests on monopiles (Sturm et al., 2008), and later interpreted through 1D (Kementzetzidis et al., 2022) and 3D FE (Solf et al., 2010) numerical simulations, respectively. A similar self-healing mechanisms has also been observed during cyclic centrifuge tests on tripod bucket foundations (Wang et al., 2018).

Pile deflection measurements are complemented by the ground monitoring data shown in Fig. 10 for the two GDP-driven MTPs. Fig. 10 displays the evolution of the total radial stress and the pore water pressure ( $\Delta\sigma_r$  and  $\Delta p_w$ ), increments with respect to post-installation values) at the soil locations and depths indicated in Fig. 2. There is evident correlation between the trends of radial soil stress and lateral pile displacement (Fig. 10(a)). Particularly, significant permanent variations in radial stress are associated with the load parcels of larger amplitude, which are also those causing the most significant lateral pile deflection. Conversely, only modest pore pressure variations have been recorded throughout the loading sequence at the considered sensor locations under the water table, which is at variance with the substantial variations that occurred during pile installation (Tsetas et al., 2023).

The above observations regarding cyclic pile–soil interaction in the presence of a gap are largely confirmed by the GDP<sub>2</sub> moment profiles shown in Fig. 11 as an example. Such profiles were derived from the FBG strain sensor data — particularly, for the first ( $N = 1$ ) and last ( $N = 1000$ ) cycles of all cyclic parcels *a* – *e* (at the corresponding maximum load level), and also for the static preloading stages preceding parcels *a* and  $e_{90}$  ( $a^{sp}$  and  $e_{90}^{sp}$  respectively, with  $F = 90$  kN, see Fig. 11(c)); circular markers and solid lines are used for the experimental data and their 4th-order polynomial interpolations, respectively.

The moment profiles seem overall to confirm that no further gap enlargement/deepening took place after the application of parcel *b*. This statement is supported by the considerable evolution of the moment profile that may be observed through parcels *a* (Fig. 11(a)) and *b* (Fig. 11(b)), whereas very limited moment variations are associated with the other cyclic parcels. The major impact of the gap on the cyclic pile response clearly emerges from the comparison in Fig. 11(b) between the moment profiles associated with the static preloading stages  $a^{sp}$  and  $e_{90}^{sp}$ . These particular profiles were selected to highlight the difference between full and partial soil–pile contact on the passive soil side — it is indeed argued that the gap had not yet been opened for  $a^{sp}$ , while the previous parcels of larger amplitude did likely prevent full contact under the  $e_{90}^{sp}$ 's low load level ( $F = 90$  kN). The latter conjecture is fully confirmed by the atypical moment distribution that is shown for  $e_{90}^{sp}$  in Fig. 11(b): the moment values down to about 3.5 m are aligned along the same linear trend that one would obtain for the case of no soil reactions and with the real lateral load eccentricity that was held during the field tests. Such a depth of 3.5 m may be regarded as a close approximation of the maximum gap depth, which is also consistent with the field observations of McAdam et al. (2020).

### 3.3. Evolution of the cyclic stiffness

The responses of GDP<sub>1</sub> and GDP<sub>2</sub> are further compared in Fig. 12 in terms of the load–displacement cycles associated with  $N = 1, 1000$  for the load parcel *a*. Comparison to the ATP monotonic curves in Fig. 6(a) is also included in the figure, which indicates good consistency in terms of (pre-gapping) pile response at the considered ATP/MTP locations.

While the cyclic responses of GDP<sub>1</sub> and GDP<sub>2</sub> appear very similar in the first cycle, appreciable differences can be noticed after 1000 cycles.

The responses of both GDP piles to slow/cyclic loading were further processed to obtain quantitative information regarding the overall cyclic stiffness. Special attention to the effects of soil–pile gapping had to be devoted when processing the experimental force–displacement cycles, such as those in Fig. 9(a). To distinguish material and geometrical non-linearity in the soil, three distinct definitions of the secant cyclic stiffness  $K_{cyc}$  were considered as per Fig. 13(a), namely with respect to (i) the initial 0.5 mm of the cyclic deflection range ( $K_{cyc}^{og}$ , at minimum load), (ii) the final 0.5 mm ( $K_{cyc}^{cg}$ , at maximum load), and (iii) the whole load/deflection range ( $K_{cyc}^{av}$ ) — it was found appropriate to determine  $K_{cyc}^{og}$  and  $K_{cyc}^{cg}$  with reference to cyclic displacement ranges of 0.5 mm (Fig. 13(a)), based on the observation that its further reduction would not alter the corresponding stiffness values. While  $K_{cyc}^{av}$  was defined to track an average secant stiffness affected both by soil plasticity and gapping (see results in Fig. 14(a)),  $K_{cyc}^{og}$  and  $K_{cyc}^{cg}$  were introduced to inspect the role of different conditions on the passive side of the pile–soil interface, i.e., in the presence of either open or (re)closed gap — hence the superscripts *og* and *cg* for ‘open-gap’ and ‘closed-gap’.

As illustrated in Fig. 14(a), the evolution of  $K_{cyc}^{av}$  against the number of cycles  $N$  clearly displays the influence of soil–pile gapping. During the main gap-opening parcels (*a* – *b*), a gradual decrease in average stiffness occurred due to the largest loading amplitudes being experienced by both GDP piles for the first time. Some slower decrease is also visible for parcel *c*, during which there was presumably no further opening of the gap. When parcel *d* (equal to *a*) was applied, the piles experienced an overall unloading and responded to cyclic loading with a permanently open gap, which explains the drop in  $K_{cyc}^{av}$  as a consequence of lateral resistance being provided only by the soil below the gap. With no further gap opening,  $K_{cyc}^{av}$  gradually increased during cycling, in a way already reported in the literature based on small-scale pile tests in dry sand (i.e., without appreciable gapping effects) (Klinkvort et al., 2010; LeBlanc et al., 2010; Abadie, 2015; Abadie et al., 2019; Richards, 2019).

To broaden the picture offered by Fig. 14(a), cyclic trends both of  $K_{cyc}^{og}$  and  $K_{cyc}^{cg}$  are plotted in Figs. 14(b)–14(c).  $K_{cyc}^{og}$  was previously introduced as representative of open-gap conditions, in which only the soil below the gap contributes to the lateral stiffness. After full formation of the gap,  $K_{cyc}^{og}$  values of approximately 27 kN/mm and 19 kN/mm may be observed at the end of parcel *b* and, very consistently, at the beginning of both parcels *d* and *e*. This outcome suggests to regard the pile-gap-soil system as a single entity in combination with the applied loading: its (current) geometrical configuration seems to determine the resulting open-gap stiffness  $K_{cyc}^{og}$ , which does explain why very similar  $K_{cyc}^{og}$  values are associated with comparable widths ( $L_x$ ) of the gap. With reference to Fig. 10(a),  $L_{x,max}$  was estimated to approximately equal  $L_x$  at the end of parcel *b* (and also at the beginning of parcels *d* – *e*), i.e., about 25.5 mm and 22.5 mm for GDP<sub>1</sub> and GDP<sub>2</sub>, respectively (see Fig. 10(a)).

The same test results are re-elaborated in Fig. 14(c) also in terms of closed-gap stiffness  $K_{cyc}^{cg}$ , which was defined to filter gapping effects out of the global pile–soil response. It is argued that, with the only exception of parcel *d*, all the other parcels allowed both piles to achieve (nearly) full contact with the resisting passive soil. With reference to the ‘full-contact parcels’, (*a*, *b*, *c*, and *e*), the  $K_{cyc}^{cg}$  values seem to align along a trend always increasing with the number of cycles, in a manner that is consistent with the pile behaviour presented in the aforementioned small-scale studies from the literature.

Overall, a good consistency between site investigation data and pile test results is confirmed by the response of GDP<sub>2</sub> featuring cyclic deflections (Fig. 10(a)) and closed-gap stiffness  $K_{cyc}^{cg}$  values (Fig. 14(c)) respectively lower and larger than GDP<sub>1</sub>'s, which reflects the larger soil density/stiffness at the GDP<sub>2</sub> location (Fig. 3).

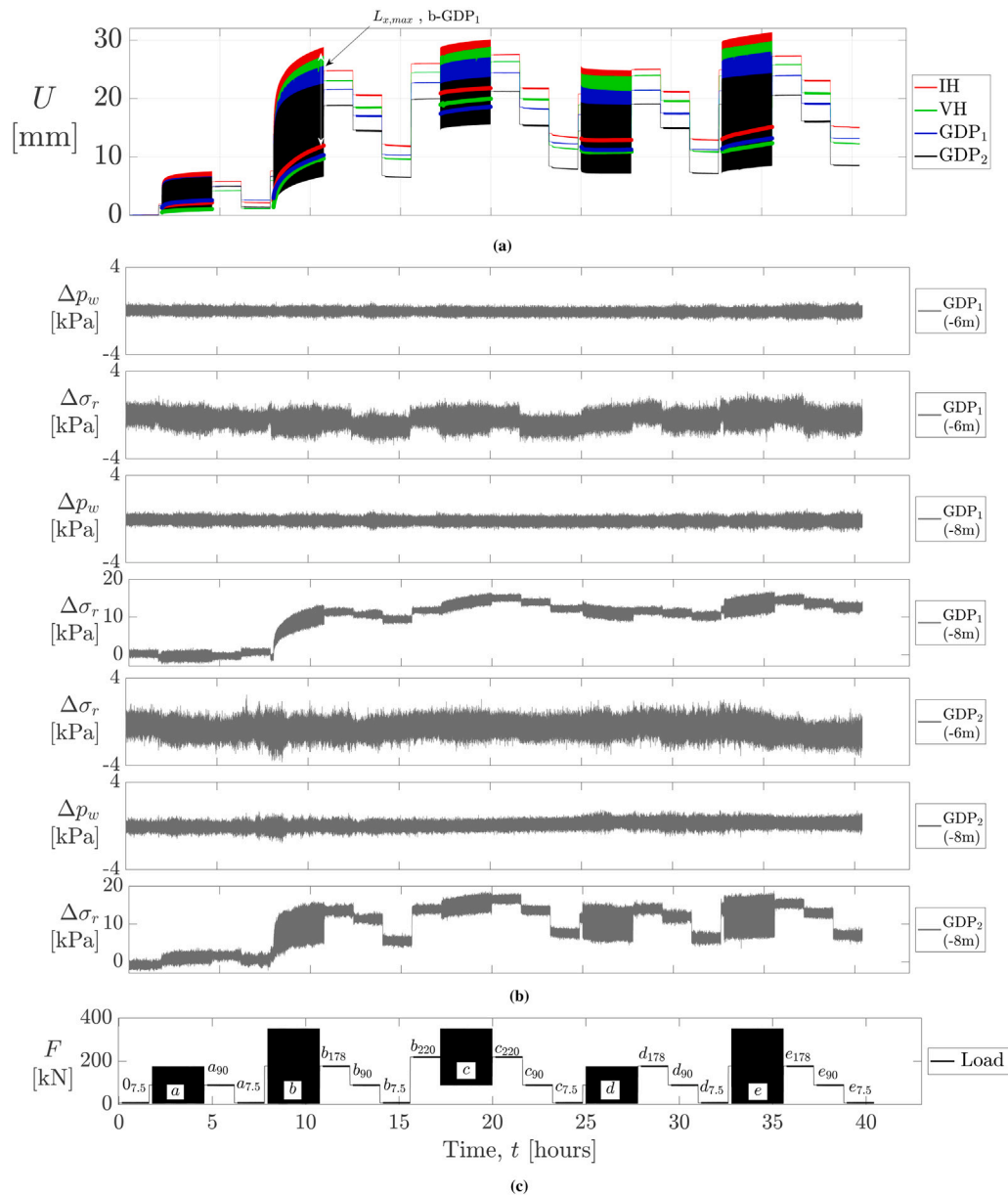


**Fig. 10.** Pile deflection and ground response recorded during the loading programme in Fig. 7: (a) lateral displacement ( $U$ ) of all MPTs (GDP<sub>1,2</sub>, IH, VH) recorded at the ground surface — the single-head arrow points to the maximum displacement experienced by GDP<sub>1</sub> at the end of parcel  $b$  ( $\approx L_{x,max}$ : maximum gap-opening over the loading programme), while the double-head arrow spans the displacement range of the IH pile at the 1000<sup>th</sup> cycle of parcel  $b$ ; (b) time increments of radial soil pressure ( $\Delta\sigma_r$ , total stress) and pore water pressure ( $\Delta p_w$ ) with respect to the initial in-situ value for GDP<sub>1</sub> and GDP<sub>2</sub> ( $\Delta\sigma_r(t=0) = \Delta p_w(t=0) = 0$ ); (c) cyclic/dynamic loading programme.

#### 4. Pile dynamics under small-amplitude load parcels

As illustrated in Fig. 7, dynamic frequency sweeps of small amplitude (2.5 kN) were interleaved between cyclic parcels. Figs. 10(a)–14 suggest altogether that weak dynamic vibrations did not impact substantially the slow/cyclic response, regardless of the larger number of applied small cycles — for instance,  $N = 17\,200$  cycles at four different values of  $F_{av}$  between parcels  $b$  and  $c$ . Generally, small-amplitude vibrations did not induce further pile deflection and gap opening.

Fig. 15 displays the evolution of (the absolute value of) the dynamic pile stiffness  $|K_{dyn}|$  during each frequency sweep. For each dynamic loading cycle,  $|K_{dyn}|$  was obtained as the ratio between the ranges of applied load (5 kN in all cases) and displacement, as illustrated in Fig. 13(b). Although all associated with small-amplitude vibrations,  $|K_{dyn}|$  values vary significantly along the sequence of f-sweeps: Particularly worth noting are the variations in  $|K_{dyn}|$  during the  $f_b$ -sweeps: while  $|K_{dyn}| \approx 20$  kN/mm when the pile was previously cycled around

$F_{av} = 90$  kN in  $a_{90}$ , a significantly larger average load of 178 kN ( $b_{178}$ ) determined a higher stiffness of about 50 kN/mm — similar conclusions also apply to the  $|K_{dyn}|$  trends during the  $f_c$ -,  $f_d$ -, and  $f_e$ -sweeps.

Fig. 16 helps to understand the observed non-monotonic relationship between  $|K_{dyn}|$  and  $F_{av}$ . The figure displays the last (1000<sup>th</sup>) load–displacement cycle associated with the main gap-opening parcels  $a$  and  $b$ , together with the dynamic responses that resulted from the  $f_a$ - and  $f_b$ -sweeps. An interesting finding emerges clearly from Fig. 16: the dynamic stiffness during individual f-sweeps seems to be strongly correlated with the (tangent) cyclic stiffness  $K_{cyc}^{tan}$  around the same  $F_{av}$  level that characterises the preceding cyclic parcel. Such a finding is more quantitatively supported, for GDP<sub>2</sub>, by Fig. 17, which shows on the left a magnified view of Fig. 15 around the  $f_b$ -sweeps and, on the right, the thousandth cycle recorded for parcel  $b$ . The cycle in Fig. 17(b) was also interpolated through a polynomial function (dotted line through the cycle), so that tangent stiffness values ( $K_{cyc}^{tan}$ , on the

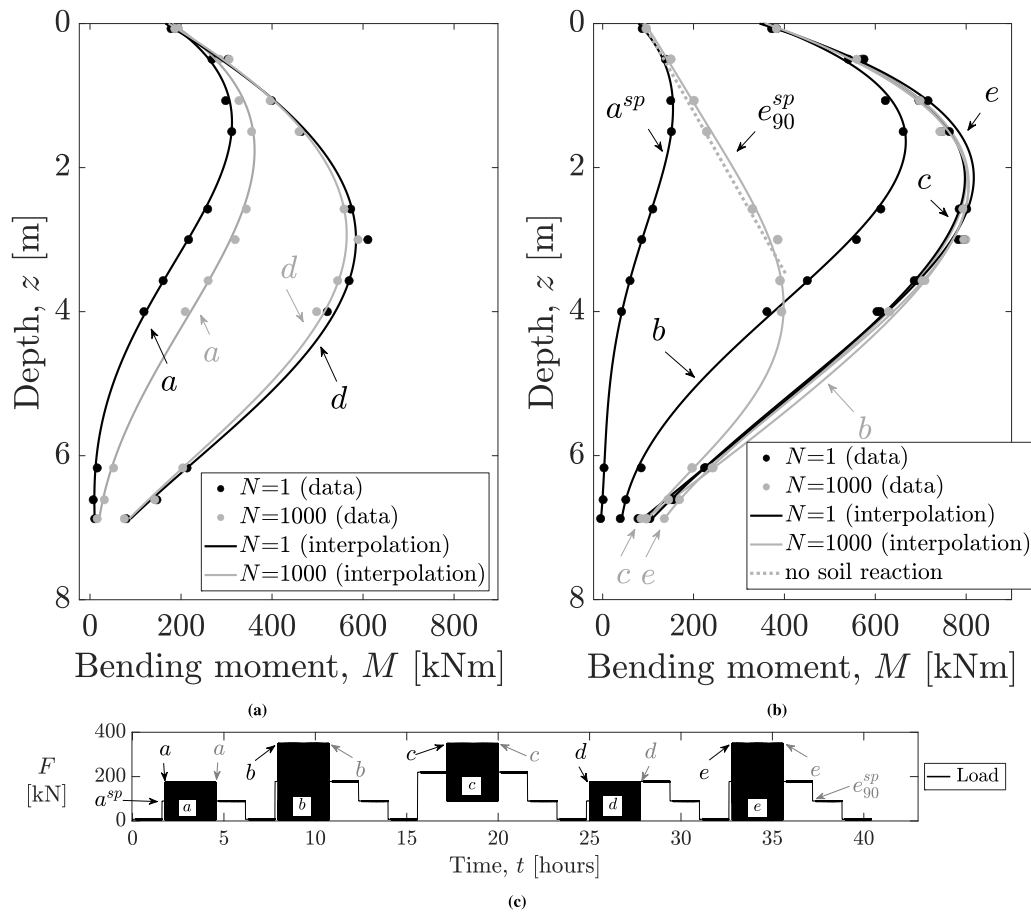


Fig. 11. (a–b) Selected GDP’s moment profiles from FBG strain sensor data and (c) their temporal correspondence with the cyclic/dynamic loading programme. Moment data (circular markers) and their 4th-order polynomial interpolations (solid lines) are plotted in (a–b) using the same colours adopted in (c).

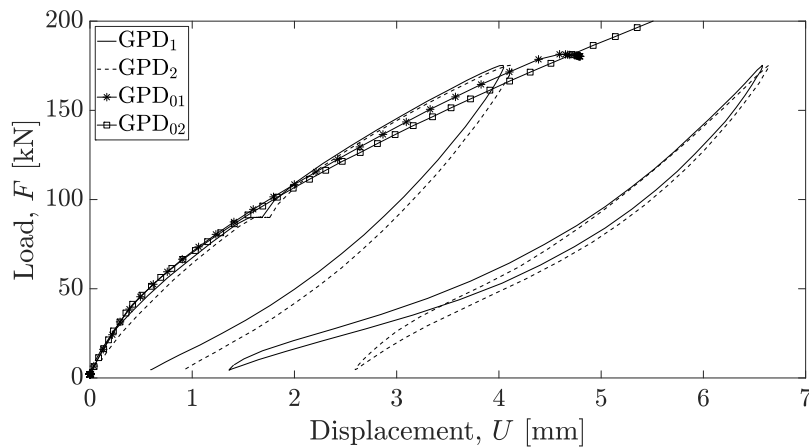


Fig. 12. GDP<sub>1</sub>-GDP<sub>2</sub> load–displacement cycles associated with  $N = 1, 1000$  for the load parcel  $a$  in Fig. 7. Monotonic test results for GDP<sub>01</sub>-GDP<sub>02</sub> (from Fig. 6(a)) are also reported for comparison.

right axis) within the relevant range of  $F_{av}$  could be readily computed through differentiation.

The comparison between Figs. 17(a) and 17(b) highlights the non-monotonic relationship between  $|K_{dyn}|$  and  $F_{av}$ , in which the  $|K_{dyn}|$  patterns in Fig. 15 follow consistently the sequence of applied  $F_{av}$  values. This observation leads to believe that a loading event of large magnitude (such as parcel  $b$ ) may provide information relevant to predicting the behaviour under subsequent small-amplitude parcels within the same load range.

$|K_{dyn}|$  appears to be nearly unaffected by the loading frequency during most of the f-sweeps applied to both piles, with the exception of  $0_{7.5}$ ,  $a_{7.5}$ ,  $b_{220}$ , and  $(b - e)_{90}$ . While some of these exceptions would not be easily explained (e.g.,  $0_{7.5}$ ,  $a_{7.5}$ , and  $b_{220}$ ), the kind of frequency-dependence observed for  $(b - e)_{90}$  has been recently interpreted by Kementzetzidis et al. (2021). Based on the results of full-scale dynamic tests, Kementzetzidis et al. showed that the low-frequency dynamics of a monopile in sand can be conveniently described through an equivalent linear visco-elastic macro-system with one degree of freedom (1dof), characterised by independent values of static stiffness

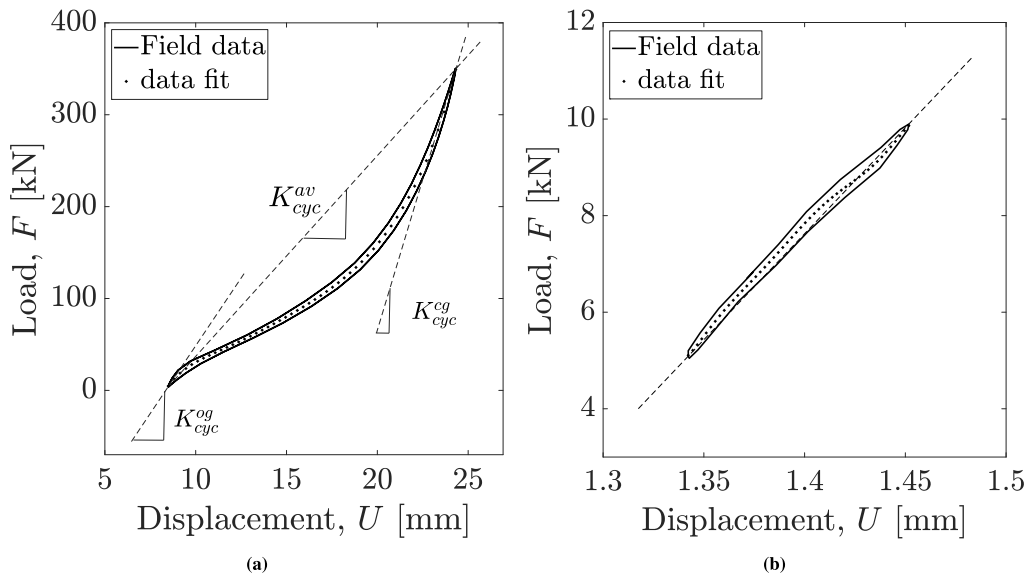


Fig. 13. Relevant definitions of (a) cyclic and (b) dynamic stiffness adopted in the discussion of pile response data.

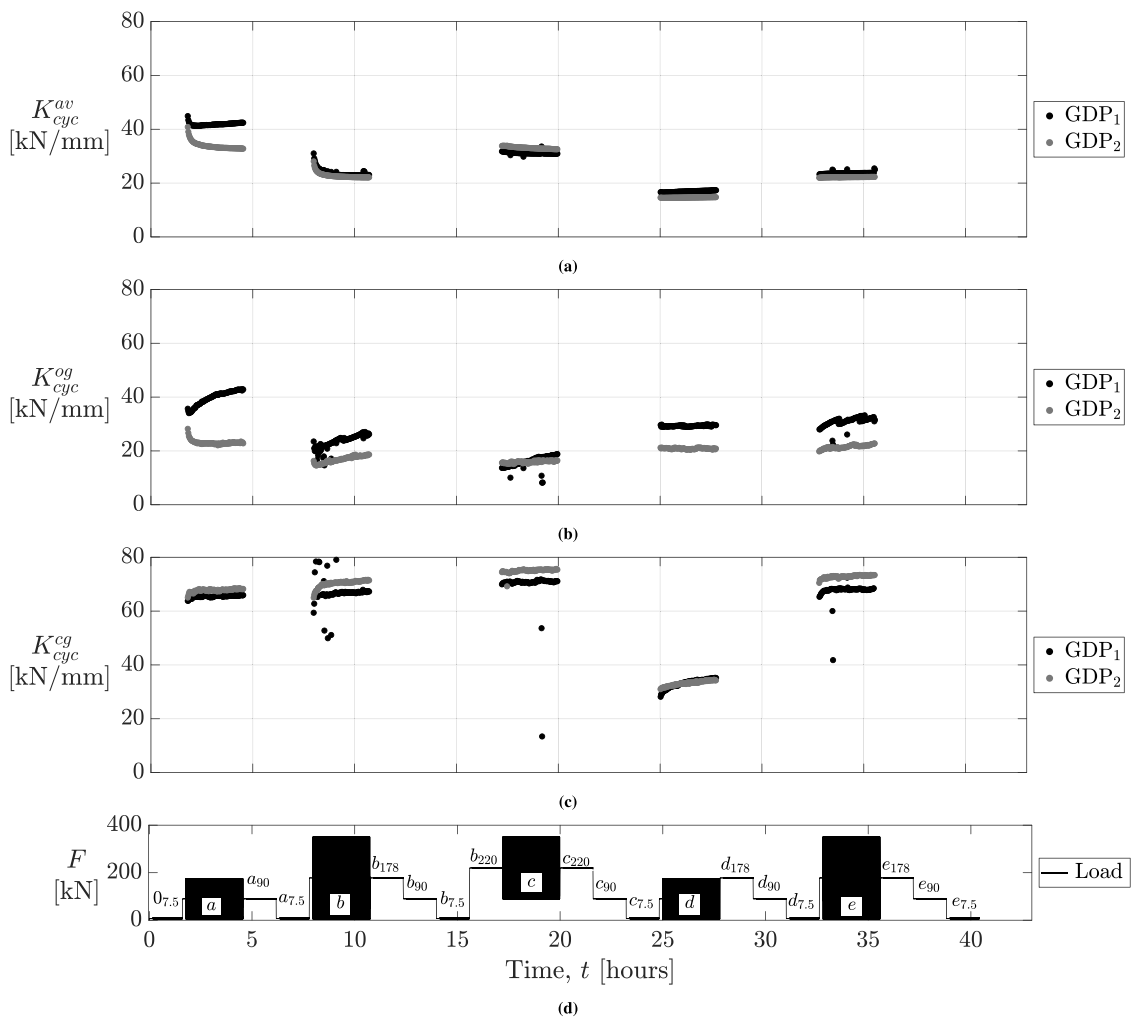


Fig. 14. Cyclic evolution vs time of the (a) average ( $K_{cyc}^{av}$ ), (b) open-gap ( $K_{cyc}^{og}$ ), and closed-gap ( $K_{cyc}^{cg}$ ) lateral pile stiffness; (d) cyclic/dynamic loading programme.

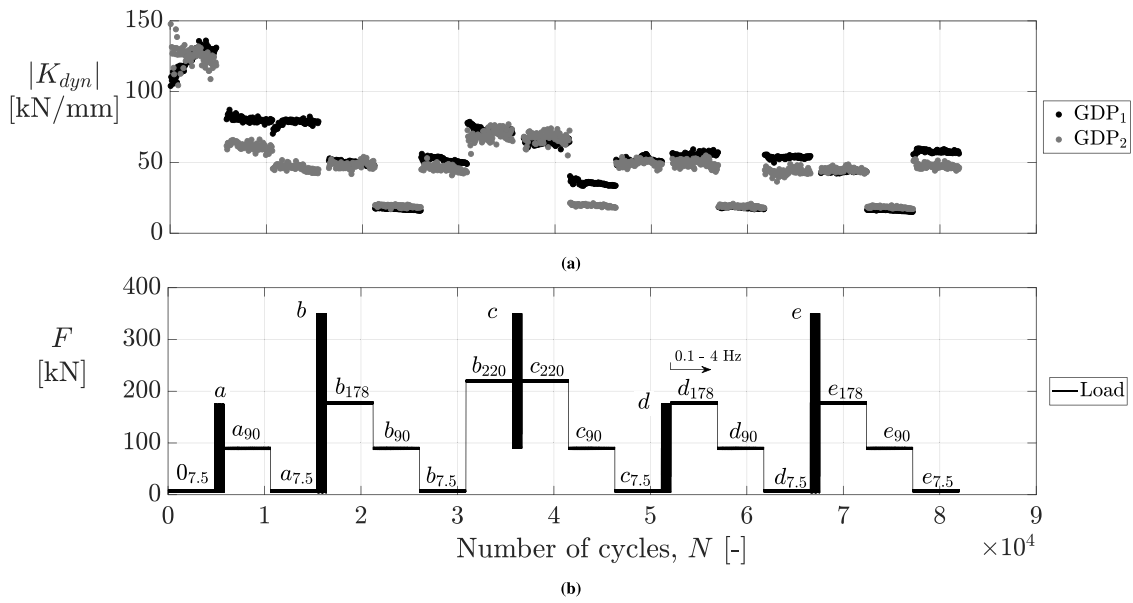


Fig. 15. (a) Absolute value of the dynamic stiffness  $|K_{dyn}|$  vs number of cycles (bottom axis) during the dynamic f-sweeps; (b) cyclic/dynamic loading programme.

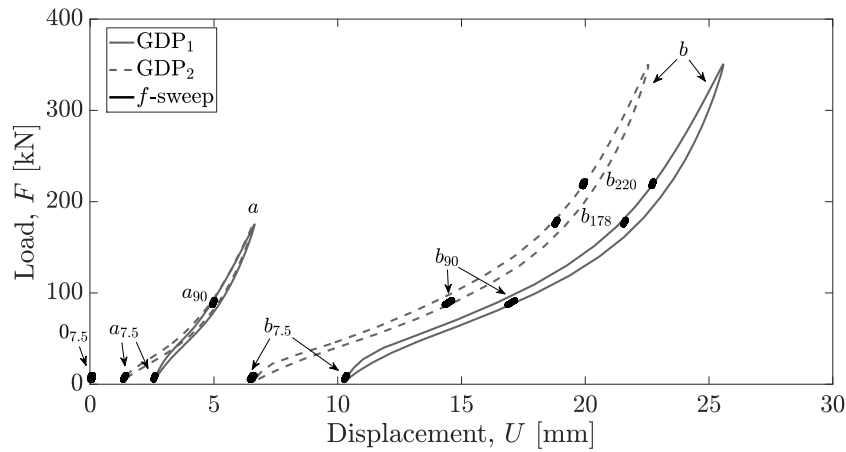


Fig. 16. Relationship between the cyclic (parcels  $a$  and  $b$ , 1000th cycles) and dynamic ( $f_a - f_b$ -sweeps) load-displacement responses for GDP<sub>1</sub> and GDP<sub>2</sub>.

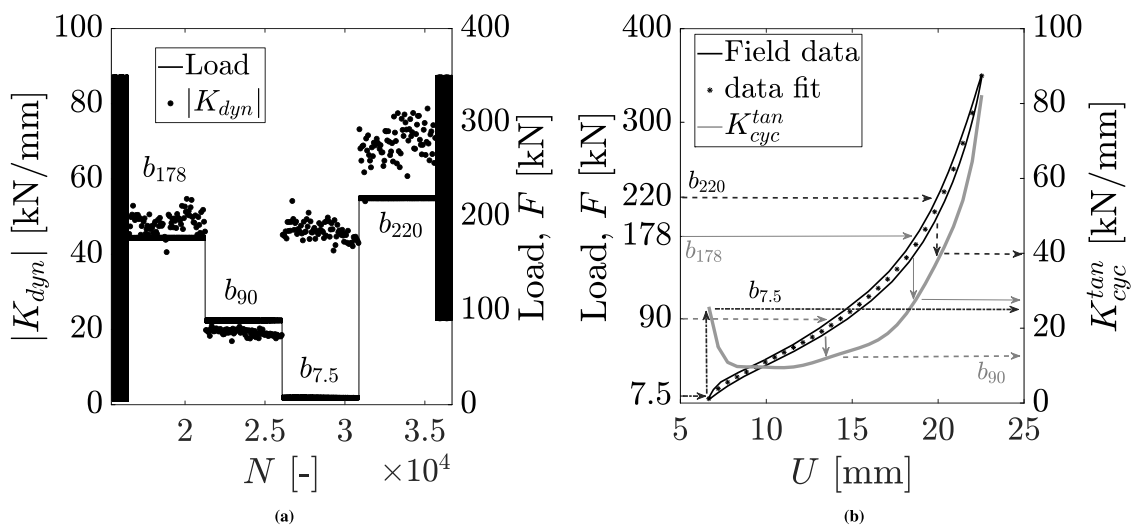


Fig. 17. Detailed comparison between GDP<sub>2</sub>'s cyclic and dynamic responses: (a) absolute value of the dynamic stiffness  $|K_{dyn}|$  (left axis) vs number of cycles at different  $F_{av}$  levels (right axis) for the frequency sweeps  $b_{7.5,90,178,220}$ ; (b) 1000th load-displacement cycle (left axis) and corresponding interpolated tangent stiffness (right axis) at the end of parcel  $b$ .

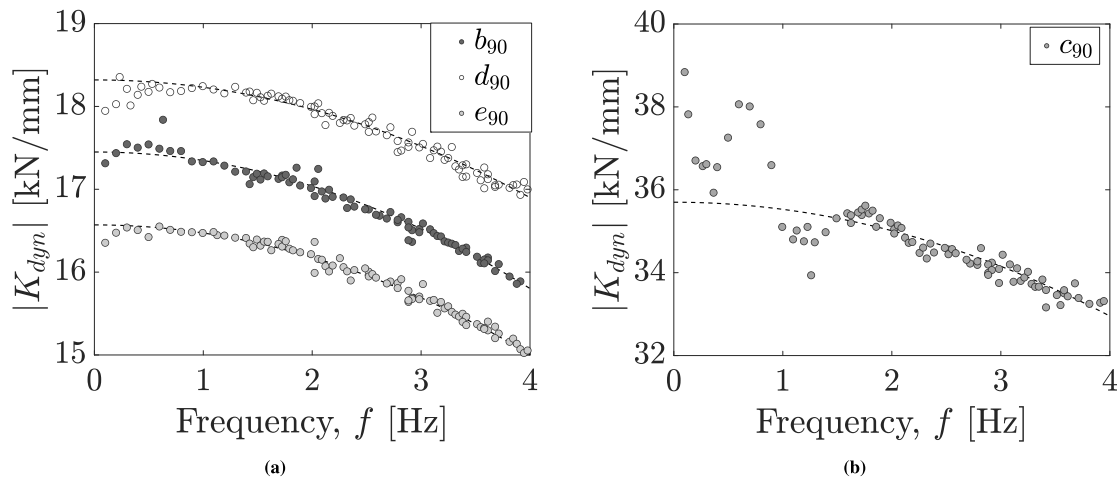


Fig. 18. Identification of the equivalent 1dof dynamic properties of the GDP<sub>1</sub>-soil system during the  $(b - e)_{90}$  f-sweeps.

Table 3

Equivalent 1dof dynamic properties identified for GDP<sub>1</sub> and GDP<sub>2</sub> with respect to different f-sweeps around  $F_{av} = 90$  kN (cf. to Fig. 18). Data associated with  $a_{90}$  did not allow the same kind of interpretation/processing — see Fig. 15.

	GDP <sub>1</sub>			GDP <sub>2</sub>		
	$K_0$ [kN/mm]	$f_{res}$ [Hz]	$\xi$ [%]	$K_0$ [kN/mm]	$f_{res}$ [Hz]	$\xi$ [%]
$a_{90}$	84	—	—	63	—	—
$b_{90}$	17.45	12.98	5%	19.92	13.41	8%
$c_{90}$	35.70	14.23	11%	20.02	12.00	9%
$d_{90}$	18.32	14.31	6%	19.95	13.71	8%
$e_{90}$	16.57	12.91	9%	18.85	12.81	12%

( $K_0$ ), damping ratio ( $\xi$ ), and undamped resonance frequency ( $f_{res}$ ). In this regard, Fig. 18(a) shows for GDP<sub>1</sub> how the experimental  $|K_{dyn}| - f$  trends emerged from  $(b, d, e)_{90}$  can be used to identify the properties of the mentioned 1dof macro-system, based on the following expression of the dynamic stiffness:

$$|K_{dyn}(f)| = K_0 \sqrt{\left[1 - \left(\frac{f}{f_{res}}\right)^2\right]^2 + \left[2\xi \frac{f}{f_{res}}\right]^2} \quad (2)$$

where  $f$  is the excitation frequency. The identified properties are summarised in Table 3 for both GDP-driven piles and the selected f-sweeps. Overall, the values provided in the table suggest that: (i) the global dynamic properties of the system are quite similar for sweeps around the same  $F_{av}$  value — with the unclear exception of  $c_{90}$  for GDP<sub>1</sub> (see Fig. 18(b)); (ii) resonance-related valleys in the  $|K_{dyn}| - f$  curves would have likely been found at significantly larger frequencies, expectedly in the order of 12–14 Hz (see identified  $f_{res}$  values in Table 3). Such dynamic macro-properties could have been more reliably identified by spanning a wider frequency range in the loading tests (Versteijlen et al., 2017; Kementzetzidis et al., 2021).

Finally, the field data were also post-processed to derive global values of foundation damping for all f-sweep stages. To this end, the following conventional definition of damping ratio ( $\xi$ ) was adopted (Jacobsen, 1960; Chopra, 1995):

$$\xi = \frac{E_D}{4\pi E_S} \quad (3)$$

where  $E_D$  and  $E_S$  denote the stored elastic energy and the plastic work (loop area) associated with individual force–displacement cycles (Yang et al., 2018). From a practical standpoint, the  $\xi$  values displayed in Fig. 19 were obtained after ‘removing’ the asymmetry introduced by the load bias  $F_{av}$  (i.e., by treating each load–displacement loop as if centred with respect to the load value  $F = F_{av}$ ). There was no need to extend the calculation procedure to the case of a ratcheting cyclic response (as

in Abadie, 2015), given the negligible displacement accumulation that was recorded during the frequency sweeps.

The damping values obtained, cycle by cycle, for both GDP-driven piles are reported in Fig. 19. In general, relatively large damping values were found, in reasonable agreement with the values alternatively identified through the stiffness–frequency trends in Fig. 18 (cf. to Table 3).

## 5. Concluding remarks

Recent research related to the GDP project (‘Gentle Driving of Piles’) has been presented in this study, which complements the companion paper by Tsetas et al. (2023). GDP is a TU Delft-led joint industry project on the development of a new vibratory driving technology for monopiles. Its stepping stone is the idea that both efficient installation and low noise emission can be achieved by applying to the pile a combination of low-frequency/axial and high-frequency/torsional vibrations. To achieve a first demonstration of the GDP concept, medium-scale field tests were performed at the sandy Maasvlakte II site in Rotterdam. Such tests included installation experiments with different driving methods (impact hammering, axial vibro-driving, and GDP driving), followed by cyclic/dynamic loading of the same piles.

The soil inhomogeneity at the Maasvlakte II site has hindered a straightforward comparison of all loading test results, and led to focus on the cyclic/dynamic response of the two GDP-driven piles — except for cyclic pile deflection data, which have been reported and compared for all the instrumented test piles.

The main experimental evidence presented in this paper may be summarised as follows:

- the measured lateral pile responses have been found to be significantly affected by the onshore geotechnical conditions at the Maasvlakte II site, especially by the occurrence of pile–soil gapping in the shallow unsaturated soil;
- the cyclic trends of lateral pile deflection have shown good compatibility with soil monitoring data, particularly with the variations in radial soil pressure that were recorded near the piles at different depths;
- while the expected pile displacement accumulation has been observed during most cyclic load parcels, both decreasing and increasing cyclic patterns have been documented for the average secant stiffness. The latter evidence has been attributed to the complex interplay of gap geometry and sand’s fabric changes under multi-amplitude cyclic lateral loading;

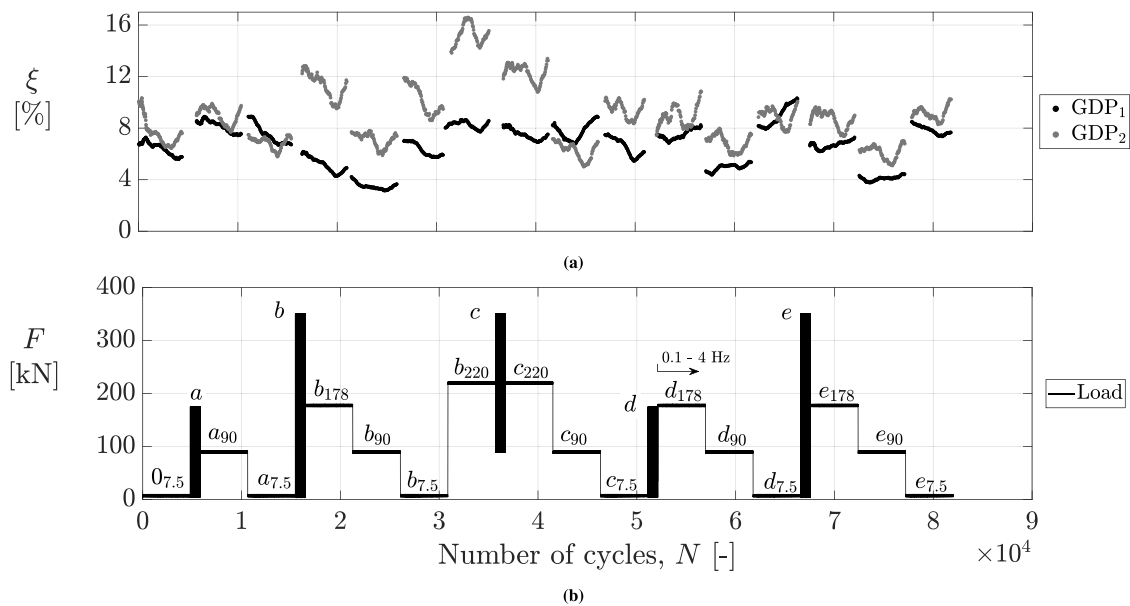


Fig. 19. Damping ratio values calculated for GDP<sub>1</sub> and GDP<sub>2</sub> from the f-sweep data.

- the lateral pile stiffness during small-amplitude frequency sweeps has been shown to be well correlated with the stiffness variations observed during the cyclic parcel of largest amplitude. The frequency sweep data have also exposed some frequency-dependence of the dynamic stiffness for loading frequencies larger than 1 Hz, and returned values of damping ratio that are broadly consistent with those alternatively inferred from dynamic stiffness-frequency trends.

In addition to the above geotechnical observations, the field campaign has preliminarily shown that not only GDP is an effective pile installation method (see companion paper), but also that it is unlikely to compromise a satisfactory post-installation response of the pile — comparing the lateral deflection trends of piles installed using different driving methods has not suggested otherwise. More quantitative analysis of all loading test results will follow based on detailed numerical modelling work.

#### CRedit authorship contribution statement

**Evangolos Kementzetzidis:** Conceptualization, Formal analysis, Data curation, Writing – original draft. **Federico Pisanò:** Conceptualization, Supervision, Writing – original draft. **Ahmed S.K. Elkadi:** Project administration, Writing – review & editing. **Apostolos Tsouvalas:** Funding acquisition, Project administration, Writing – review & editing. **Andrei V. Metrikine:** Funding acquisition, Project administration, Supervision, Writing – review & editing.

#### Declaration of competing interest

The authors declare that they have no known competing financial interests or personal relationships that could have appeared to influence the work reported in this paper.

#### Data availability

Some data may be made available upon reasonable request to the corresponding author, after approval of all GDP project partners.

#### Acknowledgements

This paper is associated with the GDP project in the framework of the GROW joint research program. Funding from Topsector Energiesubsidie van het Ministerie van Economische Zaken, Netherlands under grant number TEHE117100 and financial/technical support from the following partners is gratefully acknowledged: Royal Boskalis Westminster N.V., CAPE Holland B.V., Deltares, Netherlands, Delft Offshore Turbine B.V., Delft University of Technology, ECN, Eneco Wind B.V., IHC IQIP B.V., RWE Offshore Wind Netherlands B.V., SHL Offshore Contractors B.V., Shell Global Solutions International B.V., Sif Netherlands B.V., TNO, and Van Oord Offshore Wind Projects B.V. The important contribution to the GDP field campaign of, in alphabetical order, Rob Atkinson, Kees van Beek, Sergio S. Gómez, Timo Molenkamp, Maxim L.A. Segeren, Faraz S. Tehrani, Athanasios Tsetas, Peter de Vries, is also warmly appreciated.

#### References

- Abadie, C.N., 2015. Cyclic Lateral Loading of Monopile Foundations in Cohesionless Soils. DPhil Thesis. University of Oxford.
- Abadie, C.N., Byrne, B.W., Housby, G.T., 2019. Rigid pile response to cyclic lateral loading: laboratory tests. *Geotechnique* 69 (10), 863–876.
- Achmus, M., Schmoor, K.A., Herwig, V., Matlock, B., 2020. Lateral bearing behaviour of vibro-and impact-driven large-diameter piles in dense sand. *Geotechnik* 43 (3), 147–159.
- Albiker, J., Achmus, M., Frick, D., Flindt, F., 2017. 1 g model tests on the displacement accumulation of large-diameter piles under cyclic lateral loading. *Geotech. Test. J.* 40 (2), 173–184.
- Angelides, D.C., Roesset, J.M., 1981. Nonlinear lateral dynamic stiffness of piles. *J. Geotech. Geoenviron. Eng.* 107.
- Anusic, I., Lehane, B., Eiksund, G., Liingaard, M., 2019. Influence of installation method on static lateral response of displacement piles in sand. *Geotechnique Lett.* 9 (3), 193–197.
- Arany, L., Bhattacharya, S., Macdonald, J., Hogan, S., 2017. Design of monopiles for offshore wind turbines in 10 steps. *Soil Dyn. Earthq. Eng.* 92, 126–152.
- Barkan, D., 1967. Developments in soil dynamics. In: *International Symposium on Wave Propagation and Dynamic Properties of Earth Materials*. Univ. of New Mexico Press, pp. 599–606.
- Buckley, R.M., Byrne, B.W., Martin, S.C., McAdam, R.A., Sheil, B.B., Aghakouchak, A., Lindeboom, R., 2020. Large diameter pile testing for offshore wind applications with a focus on cyclic lateral loading and rate effects. In: Westgate, Z. (Ed.), *Frontiers in Offshore Geotechnics IV: Proceedings of the 4th International Symposium on Frontiers in Offshore Geotechnics*. ISFOG 2021, Leiden, the Netherlands: CRC Press/Balkema, pp. 1403–1412.

- Byrne, B.W., Aghakouchak, A., Buckley, R.M., Burd, H.J., Gengenbach, J., Houlsby, G.T., McAdam, R.A., Martin, C.M., Schranz, F., Sheil, B.B., Suryasentana, S.K., 2020a. PICASO: Cyclic lateral loading of offshore wind turbine monopiles. In: Westgate, Z. (Ed.), *Frontiers in Offshore Geotechnics IV: Proceedings of the 4th International Symposium on Frontiers in Offshore Geotechnics*. ISFOG 2021, Leiden, the Netherlands: CRC Press/Balkema, Houston, TX, USA, pp. 1526–1535.
- Byrne, B.W., Burd, H.J., Zdravkovic, L., Abadie, C.N., Houlsby, G.T., Jardine, R.J., Martin, C.M., McAdam, R.A., Pacheco Andrade, M., Pedro, A.M., et al., 2019. PISA design methods for offshore wind turbine monopiles. In: *Offshore Technology Conference*. Houston, TX, USA, pp. paper OTC-29373-MS.
- Byrne, B.W., McAdam, R.A., Beuckelaers, W.J., Burd, H.J., Gavin, K., Houlsby, G.T., Igoe, D.J.P., Jardine, R., Martin, C.M., et al., 2020b. Cyclic laterally loaded medium scale field pile testing for the PISA project. In: Westgate, Z. (Ed.), *Frontiers in Offshore Geotechnics IV: Proceedings of the 4th International Symposium on Frontiers in Offshore Geotechnics*. ISFOG 2021, Leiden, the Netherlands: CRC Press/Balkema, Austin, TX, USA, pp. 1323–1332.
- Chopra, A.K., 1995. *Dynamics of Structures*. Vol. 3. Prentice Hall New Jersey.
- Cuéllar, P., Baeßler, M., Rücker, W., 2009. Ratcheting convective cells of sand grains around offshore piles under cyclic lateral loads. *Granul. Matter* 11 (6), 379.
- De Nicola, A., Randolph, M.F., 1993. Tensile and compressive shaft capacity of piles in sand. *J. Geotech. Eng.* 119 (12), 1952–1973.
- Dobry, R., Gazetas, G., 1988. Simple method for dynamic stiffness and damping of floating pile groups. *Geotechnique* 38 (4), 557–574.
- Dutch Government, 2022. Offshore wind energy. [Online; Accessed Oct-2022] <https://www.government.nl/topics/renewable-energy/offshore-wind-energy>.
- Esteban, M.D., Diez, J.J., López, J.S., Negro, V., 2011. Why offshore wind energy? *Renew. Energy* 36 (2), 444–450.
- European Commission, 2020. Offshore renewable energy strategy. URL: <https://ec.europa.eu/info/law/better-regulation/have-your-say/initiatives/12517-Offshore-renewable-energy-strategy>.
- Fredlund, D.G., 2006. Unsaturated soil mechanics in engineering practice. *J. Geotech. Geoenviron. Eng.* 132 (3), 286–321.
- Frick, D., Achmus, M., 2019. Model tests on the displacement accumulation of monopiles subjected to general cyclic loading. In: Goseberg, N., Schlurmann, T. (Eds.), *Proceedings of Coastal Structures 2019*, Karlsruhe: Bundesanstalt Für Wasserbau, pp. 913–922.
- Gazetas, G., Dobry, R., 1984. Horizontal response of piles in layered soils. *J. Geotech. Eng.* 110 (1), 20–40.
- He, R., Kaynia, A.M., Zhang, J., 2019. A poroelastic solution for dynamics of laterally loaded offshore monopiles. *Ocean Eng.* 179, 337–350.
- Jacobsen, L.S., 1960. Damping in composite structures. In: *Proceedings of the Second World Conference on Earthquake Engineering*. Japan, Tokyo. Vol. 2. pp. 1029–1044, II WCEE, Tokyo, 1960.
- Jamiolkowski, M., Lo Presti, D., Manassero, M., 2003. Evaluation of relative density and shear strength of sands from CPT and DMT. In: *Soil Behavior and Soft Ground Construction*. Vol. 7. No. 119. ASCE Geotechnical Special Publication 119, pp. 201–238.
- Kagawa, T., Kraft, L.M., 1980. Lateral load-deflection relationships of piles subjected to dynamic loadings. *Soils Found.* 20 (4), 19–36.
- Kallehave, D., Byrne, B.W., LeBlanc Thilsted, C., Mikkelsen, K.K., 2015. Optimization of monopiles for offshore wind turbines. *Phil. Trans. R. Soc. A* 373 (2035), 20140100.
- Kementzetzidis, E., 2023. Cyclic behaviour of laterally loaded (mono) piles in sand - With emphasis on pile driving effects (Ph.D. thesis). Delft University of Technology.
- Kementzetzidis, E., Corciulo, S., Versteijlen, W.G., Pisanò, F., 2019. Geotechnical aspects of offshore wind turbine dynamics from 3D non-linear soil-structure simulations. *Soil Dyn. Earthq. Eng.* 120, 181–199.
- Kementzetzidis, E., Metrikine, A.V., Versteijlen, W.G., Pisanò, F., 2021. Frequency effects in the dynamic lateral stiffness of monopiles in sand: insight from field tests and 3D FE modelling. *Geotechnique* 71 (9), 812–825.
- Kementzetzidis, E., Pisanò, F., Metrikine, A.V., 2022. A memory-enhanced  $p-y$  model for piles in sand accounting for cyclic ratcheting and gapping effects. *Comput. Geotech.* 148, 104810.
- Kementzetzidis, E., Pisanò, F., Tsetas, A., Metrikine, A.V., 2023. Gentle Driving of Piles (GDP) at a sandy site combining axial and torsional vibrations: quantifying the influence of the pile installation method on the response to lateral loading. Under review.
- Klinkvort, R.T., 2012. *Centrifuge Modelling of Drained Lateral Pile-Soil Response* (Ph.D. thesis). The Technical University of Denmark, DTU Civil Engineering.
- Klinkvort, R.T., Leth, C.T., Hededal, O., 2010. Centrifuge modelling of a laterally cyclic loaded pile. In: Springman, S., Laue, J., Steward, L. (Eds.), *Proceedings of the 7th International Conference on Physical Modelling in Geotechnics*. ICPMG 2010, Taylor & Francis London, Zurich, Switzerland, London, UK, pp. 959–964.
- Koschinski, S., Lüdemann, K., 2013. Development of noise mitigation measures in offshore wind farm construction. In: *Commissioned By the Federal Agency for Nature Conservation*. pp. 1–102.
- Lammertz, P., 2003. Field studies on bearing capacity of vibratory and impact driven piles. In: *International Young Geotechnical Engineers' Conference*. IYGEC, Mamaia, Romania.
- Lazari, M., Sanavia, L., di Prisco, C., Pisanò, F., 2019. Predictive potential of Perzyna viscoplastic modelling for granular geomaterials. *Int. J. Numer. Anal. Methods Geomech.* 43 (2), 544–567.
- LeBlanc, C., Houlsby, G., Byrne, B., 2010. Response of stiff piles in sand to long-term cyclic lateral loading. *Geotechnique* 60 (2), 79–90.
- Li, W., Igoe, D., Gavin, K., 2015. Field tests to investigate the cyclic response of monopiles in sand. *Proc. Inst. Civ. Eng. Geotech. Eng.* 168 (5), 407–421. <http://dx.doi.org/10.1680/jgeen.14.00104>.
- Liu, H., Kementzetzidis, E., Abell, J.A., Pisanò, F., 2022. From cyclic sand ratcheting to tilt accumulation of offshore monopiles: 3D FE modelling using SANISAND-MS. *Geotechnique* 72 (9), 753–768.
- Matlock, H., 1970. Correlations for design of laterally loaded piles in soft clay. In: *Proceedings of 2nd Offshore Technology Conference*, Houston, TX, USA. 1, pp. 577–594.
- Matlock, H., Foo, S., Bryant, L., 1978. Simulation of lateral pile behavior. In: *Proceedings of the ASCE Geotechnical Engineering Division Specialty Conference*. Vol. 1. Pasadena, CA, USA, pp. 600–619.
- Matlock, H., Reese, L.C., 1962. Generalized solutions for laterally loaded piles. *Trans. Am. Soc. Civ. Eng.* 127 (1), 1220–1247.
- Mazza, N., Holeyman, A., 2019. Frequency-penetration response spectrum on vibratory amplitude matching of monopiles. In: Bullock, P., Verbeek, G., Tara, D., Paikowsky, S. (Eds.), *10th International Conference on Stress Wave Theory and Testing Methods for Deep Foundations*. ASTM International, San Diego, California, USA.
- McAdam, R.A., Byrne, B.W., Houlsby, G.T., Beuckelaers, W.J., Burd, H.J., Gavin, K.G., Igoe, D.J., Jardine, R.J., Martin, C.M., Muir Wood, A., et al., 2020. Monotonic laterally loaded pile testing in a dense marine sand at Dunkirk. *Geotechnique* 70 (11), 986–998.
- McClelland, B., Focht, J., 1956. Soil modulus for laterally loaded piles. *J. Soil Mech. Found. Div.* 82 (4), 1–22.
- Meijers, P., Tsouvalas, A., Metrikine, A., 2018. A non-located method to quantify plastic deformation caused by impact pile driving. *Int. J. Mech. Sci.* 148, 1–8.
- Metrikine, A., Tsouvalas, A., Segeren, M., Elkadi, A., Tehrani, F., Gómez, S., Atkinson, R., Pisanò, F., Kementzetzidis, E., Tsetas, A., Molenkamp, T., van Beek, K., P, D., 2020. GDP: a new technology for Gentle Driving of (mono)Piles. In: Westgate, Z. (Ed.), *Frontiers in Offshore Geotechnics IV: Proceedings of the 4th International Symposium on Frontiers in Offshore Geotechnics*. ISFOG 2021, Leiden, the Netherlands: CRC Press/Balkema, Austin, TX, USA, pp. 736–745.
- Minister of Economic Affairs and Climate Policy, 2020. Offshore wind energy roadmap 2030. URL: <https://www.government.nl/topics/renewable-energy/documents/parliamentary-documents/2018/03/27/letter-to-parliament-offshore-wind-energy-roadmap-2030>.
- Mosher, R.L., 1987. Comparison of Axial Capacity of Vibratory-Driven Piles to Impact-Driven Piles. Technical Report, Engineer Research and Development Center (ERDC).
- Mosher, R.L., 1990. Axial capacity of vibratory-driven piles versus impact-driven piles. *Transp. Res. Rec.* (1277).
- Mylonakis, G., Gazetas, G., 1999. Lateral vibration and internal forces of grouped piles in layered soil. *J. Geotech. Geoenviron. Eng.* 125 (1), 16–25.
- Novak, M., 1974. Dynamic stiffness and damping of piles. *Can. Geotech. J.* 11 (4), 574–598.
- OpenStreetMap contributors, 2017. Planet dump retrieved from <https://planet.osm.org>. URL: <https://www.openstreetmap.org>.
- Page, A.M., Norén-Cosgriff, K., Skau, K.S., Kaynia, A.M., 2019. REDWIN foundation models for integrated dynamic analyses of offshore wind turbines. In: *International Conference on Offshore Mechanics and Arctic Engineering*. Vol. 58899. American Society of Mechanical Engineers, V010T09A073.
- Pisanò, F., Askarinejad, A., Wang, H., Maghsoodi, S., Gavin, K.G., Segeren, M.L.A., Elkadi, A.S.K., de Lange, D., Konstadinou, M., 2022a. MIDAS: Monopile improved design through advanced cyclic soil modelling. In: *Proceedings of 20th International Conference on Soil Mechanics and Geotechnical Engineering*. ICSMGE2022, Sydney, Australia.
- Pisanò, F., Liu, H., Kementzetzidis, E., 2022b. Geotechnical modelling framework for the tilting analysis of offshore monopiles under environmental cyclic loading. In: Sharman, K., Myers, A., Roddier, D. (Eds.), *Proceedings of the ASME 2022 International Offshore Wind Technical Conference (IOWTC2022)*. IOWTC2022, Boston, 2022.
- Poulos, H.G., 1971. Closure of "behavior of laterally loaded piles: I-single piles". *J. Soil Mech. Found. Div.* 98, 1269–1271.
- Poulos, H.G., Davis, E.H., 1980. *Pile Foundation Analysis and Design*. Monograph.
- Ramírez, L., Fraile, D., Brindley, G., 2021. Offshore wind in Europe: Key trends and statistics 2020. *WindEurope*.
- Reese, L.C., Cox, W.R., Koop, F.D., et al., 1975. Field testing and analysis of laterally loaded piles on stiff clay. In: *Offshore Technology Conference*. Offshore Technology Conference.
- Richards, I., 2019. *Monopile Foundations Under Complex Cyclic Lateral Loadings* (Ph.D. thesis). University of Oxford.
- Richards, I., Bransby, M., Byrne, B., Gaudin, C., Houlsby, G., 2021. Effect of stress level on response of model monopile to cyclic lateral loading in sand. *J. Geotech. Geoenviron. Eng.* 147 (3), 04021002.

- Rodger, A., Littlejohn, G., 1980. A study of vibratory driving in granular soils. *Géotechnique* 30 (3), 269–293.
- Rudolph, C., Bienen, B., Grabe, J., 2014. Effect of variation of the loading direction on the displacement accumulation of large-diameter piles under cyclic lateral loading in sand. *Can. Geotech. J.* 51 (10), 1196–1206.
- Shadlou, M., Bhattacharya, S., 2014. Dynamic stiffness of pile in a layered elastic continuum. *Geotechnique* 64 (4), 303.
- Shadlou, M., Bhattacharya, S., 2016. Dynamic stiffness of monopiles supporting offshore wind turbine generators. *Soil Dyn. Earthq. Eng.* 88, 15–32.
- Solf, O., Kudella, P., Triantafyllidis, T., 2010. Investigation of the self-healing effect of monopile foundations. In: Springman, S., Laue, J., Seward, L. (Eds.), *International Conference on Physical Modelling in Geotechnics. ICPMG*, London, UK: CRC Press, Zurich, Switzerland, pp. 1003–1008.
- Staubach, P., Machaček, J., Bienen, B., Wichtmann, T., 2022. Long-term response of piles to cyclic lateral loading following vibratory and impact driving in water-saturated sand. *J. Geotech. Geoenviron. Eng.* 148 (11), 04022097.
- Stehly, T.J., Beiter, P.C., 2020. 2018 Cost of Wind Energy Review. Technical Report, National Renewable Energy Lab.(NREL), Golden, CO (United States).
- Sturm, H., Solf, O., Kudella, P., 2008. Self-healing effects of shallow foundations for offshore wind turbine structures. In: Mlynarek, Z. (Ed.), *11th Baltic Sea Geotechnical Conference: "Geotechnics in Maritime Engineering"*. Gdansk, Poland, pp. 301–308.
- Truong, P., Lehane, B., Zania, V., Klinkvort, R.T., 2019. Empirical approach based on centrifuge testing for cyclic deformations of laterally loaded piles in sand. *Géotechnique* 69 (2), 133–145.
- Tsetas, A., Gómez, S.S., Tsouvalas, A., van Beek, K., Tehrani, F.S., Kementzetzidis, E., Pisanò, F., Elkadi, A., Segeren, M., Molenkamp, T., Metrikine, A.V., 2020. Experimental identification of the dynamic behaviour of pile-soil system installed by means of three different pile-driving techniques. In: Papadarakakis, M., Fragiadakis, M., Papadimitriou, C. (Eds.), *Proceedings of the XI International Conference on Structural Dynamics. Vol. II. EURODDYN 2020*, European Association for Structural Dynamics, Athens, Greece, pp. 3005–3015.
- Tsetas, A., Tsouvalas, A., Gómez, S., Pisanò, F., Kementzetzidis, E., Molenkamp, T., Elkadi, A., Metrikine, A., 2023. Gentle driving of piles GDP at a sandy site combining axial and torsional vibrations: part I – installation tests. *Under Rev. Ocean Eng.*
- Tsouvalas, A., 2020. Underwater noise emission due to offshore pile installation: A review. *Energies* 13 (12), 3037.
- Tsouvalas, A., Metrikine, A., 2016a. Noise reduction by the application of an air-bubble curtain in offshore pile driving. *J. Sound Vib.* 371, 150–170.
- Tsouvalas, A., Metrikine, A.V., 2016b. Structure-borne wave radiation by impact and vibratory piling in offshore installations: From sound prediction to auditory damage. *J. Mar. Sci. Eng.* 4 (3), 44.
- Versteijlen, W., Renting, F., van der Valk, P., Bongers, J., van Dalen, K., Metrikine, A., 2017. Effective soil-stiffness validation: Shaker excitation of an in-situ monopile foundation. *Soil Dyn. Earthq. Eng.* 102, 241–262.
- Vos, P., 2015. Origin of the Dutch Coastal Landscape: Long-Term Landscape Evolution of the Netherlands During the Holocene, Described and Visualized in National, Regional and Local Palaeogeographical Map Series. *Barkhuis*.
- Wang, H., Lehane, B., Bransby, M., Askarinejad, A., Wang, L., Hong, Y., 2022. A simple rotational spring model for laterally loaded rigid piles in sand. *Mar. Struct.* 84, 103225.
- Wang, L., Wang, H., Zhu, B., Hong, Y., 2018. Comparison of monotonic and cyclic lateral response between monopod and tripod bucket foundations in medium dense sand. *Ocean Eng.* 155, 88–105.
- Wu, X., Hu, Y., Li, Y., Yang, J., Duan, L., Wang, T., Adcock, T., Jiang, Z., Gao, Z., Lin, Z., et al., 2019. Foundations of offshore wind turbines: A review. *Renew. Sustain. Energy Rev.* 104, 379–393.
- Yang, H., Sinha, S.K., Feng, Y., McCallen, D.B., Jeremić, B., 2018. Energy dissipation analysis of elastic-plastic materials. *Comput. Methods Appl. Mech. Engrg.* 331, 309–326.
- Zhu, B., Li, T., Xiong, G., Liu, J.C., 2016. Centrifuge model tests on laterally loaded piles in sand. *Int. J. Phys. Model. Geotech.* 16 (4), 160–172.